Pro Gradu

Selective trapping of oligos to triangular gold nanoparticles utilizing dielectrophoresis

Tanja Andrejeff

17th April 2014

UNIVERSITY OF JYVÄSKYLÄ
NANOSCIENCE CENTER
DEPARTMENT OF PHYSICS
MOLECULAR ELECTRONICS AND PLASMONICS

Preface

The work reported in this Master's thesis has been carried out at Nanoscience Center at the Department of Physics in the University of Jyväskylä between June 2013 and February 2014.

I would like to thank my supervisors, Dr. Jussi Toppari for giving me an opportunity to work in Molecular electronics and Plasmonics group and PhD. students Boxuan Shen and Kosti Tapio for providing me practical guidance into molecular electronics. Thanks for Your trust in me and encouragement throughout my time at Nanoscience Center. I would also like to thank staff and students of Nanoscience Center for collegian support, friendship and sharing their knowledge whenever I needed it.

Finally, I wish to thank my parents and siblings, and my dear friends for supporting me throughout my studies and helping me, at times, to detach my thoughts from the busy life of a student. You all are irreplaceable in my life.

Jyväskylä 17th April 2014

Tanja Andrejeff

Abstract

Triangular shaped particles are an interesting research topic since there are three plasmonically active tips, which can be utilized in new molecular sensing application systems. In this research we used dielectrophoretic force to trap thiol-modified (5'-end) and Cy3-dye-labeled (3'-end) single-stranded DNA (ssDNA) oligonucleotides, size 40 nt (about 22 nm long), to the corners of the gold triangles. These gold triangles were 20 nm thick and side length was 1 µm. The trapping experiment was done under AC-circuit and the gathering of the oligos to the triangles was studied in situ under confocal microscope. The theoretical values for dielectrophoretic force with different voltages were simulated with finite element method. Experimentally the required DEP-force was achieved by using about 40 V_{pp} voltage and in the simulation system with 34 V_{pp}. Most of the oligos formed "cloud" around the triangle and few of them trapped also on the corners. This "cloud" can be seen also in simulations, where the gathering of the oligos was modeled. At least, our research prove that gold triangles can be used for trapping biomolecules and hence also to sensing and detecting them.

Key words:
DEP force, fluorescent, gold, oligo, trapping, triangle

Tiivistelmä

Nykyinen yhteiskunta osaa olla vaativa: haluamme sisällyttää mahdollisimman paljon erilaisia toimintoja yhteen pieneen laitteeseen ilman, että laitteen kokoa joudutaan suurentamaan. Tämän haasteen myötä varsinkin elektroniikan ala on kohdannut jatkuvasti uusia haasteita kehitellessään uusia tekniikoita rakentaa yhä pienempiä komponentteja. Nanoteknologian myötä on siirrytty mikroskaalan komponenteista nanoskaalan komponentteihin, mutta nyt nykyiset litografiatekniikat ovat kohdanneet rajansa ja ilman uutta tekniikkaa pienempään ei pystytä menemään. Siksipä, viime aikoina on kehitelty uusia tekniikoita, joidenka avulla voidaan liittää yksittäisiä molekyylejä ja atomeja osaksi pienempiä rakennelmia. Puhutaan molekyylielektroniikasta. Esimerkiksi sähköpiirien osiksi voitaisiin liittää biomolekyylejä, jotka voisivat toimia yksittäisten komponenttien/johdinten rooleissa.

Yksi mielenkiintoisimmista molekyyleistä on DNA-molekyyli. Se on joustava ja helposti muokattavissa oleva molekyyli. Tämän lisäksi sen loistava itsejärjestäytymiskyky avaa paljon uusia mahdollisuuksia rakennella aivan uudenlaisia nanoskaalan rakennelmia. Tästäpä hyvänä esimerkkinä on Paul Rothemundin valmistamat DNA-origami-rakennelmat, joita voidaan esimerkiksi käyttää rakennustelineinä monimutkaisemmille nanorakennelmille.

Tässä opinnäytetyössä tioliryhmällä varustettuja oligonukleotideja loukutettiin selektiivisesti kolmionmuotoisten kultananopartikkelien kärkiin. Oligonukleotidi eli oligo on lyhyt yksijuosteinen DNA-molekyyli, johon voidaan liittää tioliryhmä ja fluoresoiva merkkimolekyyli. Tämän tutkimuksen oligonukleotidi sisältää 40 nukleotidia ja se on noin 22 nm pitkä. Merkkimolekyyleinä käytettiin Cy3- ja Cy5-värimolekyylejä.

Dielektroforeesissa käytettiin korkeataajuisia sähkökenttiä (MHz) ohjaamaan oligoja korkeampien sähkökentän gradienttien alueille (kolmioiden kärjet). Näissä paikoissa oligot muodostivat tioliryhmien avulla kovalenttisen sidoksen kolmion kulta-atomien kanssa ja näin ollen pystyivät tarrautumaan kolmioon kiinni. Tämän loukutus prosessin onnistumista tarkasteltiin fluoresenssikuvantamisella ja laserskannerilla varustetun konfokaalimikroskoopin avulla.

Numeerisesti dielektroforeesia simuloitiin käyttämällä elementtimenetelmää, jonka avulla arvioitiin jännitteen minimiarvo, jolla saataisiin tuotettua tarpeeksi suuri

dielektrinen voima vaimentamaan oligomeerien Brownin liikkeen vaikutusta ja ohjaamaan oligot vain kolmion kärki alueille. Numeerisesti arvioimalla riittävän suuri dielektrinen voima kolmion kärki alueille saavutettaisiin 34 V_{pp} avulla. Kun taas kokeellisesti tämä jännitteen arvo ei vielä riittänyt ohjaamaan oligoja kolmion kärkiin, vaan jännitteeksi tarvittiin 40 V_{pp}.

Tässä opinnäytetyössä käytettiin kolmion muotoisia kultananopartikkeleita, jotka olivat 20 nm ohuita ja joiden sivut olivat 1 µm pituisia. Kolmion muotoisista partikkeleista mielenkiintoisia tekee se, että niillä on kolme sähköisesti aktiivista kärkeä. Tälle ominaisuudelle voisi löytyä mahdollisia sovelluskohteita mm. rakennettaessa uudenlaisia molekyylisensoreita.

List of Abbreviations

3' end of ssDNA	phosphate end -group linked to 3rd carbon in the sugar
5' end of ssDNA	hydroxyl end -group linked to 5th carbon in the sugar
A	adenine
AC	alternating current
ACEO	AC electro-osmotic
AFM	atomic force microscopy
AuNPs	gold nanoparticles
bp	base pair(s)
C	cytosine
Cy3	fluorescent cyanine dye, emission maximum $\sim$ 570 nm
Cy5	fluorescent cyanine dye, emission maximum $\sim$ 650-670 nm
DC	direct current
DCA	dichloroacetic acid
DEP	dielectrophoresis
DFT	density functional theory
DI	de-ionized
DMT	dimethoxytrityl
DNA	deoxyribonucleic acid
dsDNA	double-stranded DNA
DTT	dithiothreitol
EBL	electron beam lithography
EDL	electrical double layer
ET	electrothermal
FEM	finite element method
G	guanine
HPLC	high-performance liquid chromatography
IDT	Integrated DNA Technologiest company
MD	molecular dynamics
NSC	Nanoscience Center of University of Jyväskylä, Finland
nt	nucleotide(s)
oligo	DNA oligonucleotide, i.e, short ssDNA molecule

pp	peak-to-peak
QM	quantum mechanics
RIE	reactive-ion etcher
rms	root mean square
RNA	ribonucleic acid
SAMS	self-assembled monolayers
SEM	scanning electron microscope
ssDNA	single-stranded DNA
STM	scanning tunneling microscopy
T	thymine
TCA	trichloroacetic acid
UHV	ultra-hight vacuum

Contents

Introduction

The concept of molecular electronics was born in 1974, when Mark Ratner ("father of the molecular-scale electronics") suggested connecting the molecules into an electrical circuit. After his suggestion there has been many studies of connecting molecules to electric circuits. Especially, it has been examined how to attach biomolecules to gold surface [1].

Few years after birth of the concept of molecular electronics self-assembled monolayers (SAMS) were discovered. It was observed, that molecules with thiol groups on gold surface can self-assemble into individual or monolayers. Since, it has been tried to find use for these kind of structures and one application is to use them for building molecular-based electronic devices, biosensors and new types of optical materials [2].

The bio-inorganic architectures at the nanoscale started, when Chad Mirkin and Robert Letsinger, in 1996, reported that they have begun to use DNA and gold colloids to assemble inorganic materials [3]. This discovery not yet caused mass popularity, but once Paul Rothemund, in 2006, presented the first DNA-origami structures, the popularity of bio-electronics started to increase exponentially [4]. These structures are based on the ability of DNA molecules to be joined together and bind other molecules to themselves. Due to that they can be act as a scaffold for complex nanomachines. These structures are also examined here at the University of Jyväskylä.

This thesis examines the use of triangular gold nanoparticles in molecular electronics. At first, this thesis introduce some theoretical basics of DNA, oligonucleotides, dielectroforesis and fluid dynamics in nanoelectrode system and then in the second chapter, experimental method of trapping oligos to triangular gold nanoparticles and the result of experiments and simulations are described.

Part I

Theory

Chapter 1

DNA and oligonucleotides

1.1 Deoxyribonucleic acid

DNA alias deoxyribonucleic acid is a polynucleotide, which forms the 3-dimensional structure of genetic material. It is a linear polymer, which consist of smaller subunits, nucleotides. These subunits consist of nitrogenous base, sugar and phosphate groups. Nitrogenous bases can be divided to pyrimidines and purines. Pyrimidines are cytosine (C) and thymine (T) and purines are guanine (G) and adenine (A). Pentose sugar is a D-deoxyribose. DNA is a polymer of nucleotides, where phosphodiester linkages the 5'-hydroxyl group of one pentose and the 3'-hydroxyl group of the next together. DNA can appear as a single-stranded (ssDNA) or double-stranded (dsDNA) form. Short nucleotide acid, which has 50 or less nucleotides are generally called oligonucleotides. A longer nucleotide acid is called a polynucleotide. In a double-stranded form, parallel nucleotides form nucleotide pairs by using hydrogen bonds. There are two hydrogen bonds between adenine and thymine and three between guanine and cytosine (See Fig. 1.1). A secondary structure of dsDNA is double helix, because it is energetically most favorable form [5].

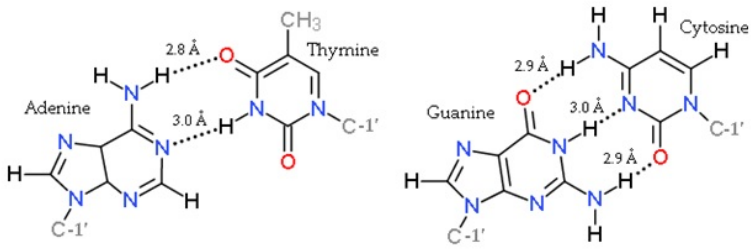

Figure 1.1: Hydrogen bonds between nitrogenous bases. There is a covalent bond between nitrogenous base and C-1' carbon of the pentose sugar [5].

1.2 Oligonucleotides

Oligonucleotides , oligomer or oligos are short sequences of DNA or RNA strands. This short synthetic piece of DNA can be used to bind or find its matching sequence even in a complex mixture of millions of unrelated pieces of DNA. This helps researchers to study and decode the genetic sequence of different living organism. Other interesting application to use oligos is to use them to be part of the molecular electronics devices, where usually oligo is attached to gold with thiol-group [6, 7].

There are many ways to synthesize oligonucleotides and one method is to use phosphoramidites. The first step is to remove dimethoxytrityl (DMT) group with solution of acid, such as 2% trichloroacetic acid (TCA) or 3% dichloroacetic acid (DCA), in an inert solvent (dichloromethane or toluene). The second step is to activate deoxynucleoside phosphoramidite solution with solution of tetrazole catalyst and add this to previous solution. 5'-hydroxy group reacts with the activated phosphoramidite moiety of the incoming nucleoside phosphoramidite to form a phosphite triester linkage. The third step is to use acetic anhydride in pyridine to acylate any unreactive nucleoside and to remove phosphite adducts from the bases. After this, it is oxidized with iodine in aqueous lutidine, which converts the phosphite internucleotide linkage to phosphate. The next step is again to remove dimethoxytrityl group and do the same cycle to add more nucleotide to get longer oligo. Before third step, sulfurization can also be done, which do not need oxidation step after capping step. In this case, oligonucleotide with phosphorothioates can be obtain. See synthesis cycle in Appendix A.1 [7].

After synthesis, oligonucleotides are analyzed and purified by using high-performance liquid chromatography (HPLC), which can be divided to anion-exchange HPLC and reversed-phase HPLC. In anion-exchange HPLC, the oligonucleotides are separated by using charge differences and in reversed-phase HPLC, the oligonucleotides are separated by using differences in hydrophobicity [7, 8].

In some applications oligonucleotides must be labeled, so that its presence can be identified. Oligos can be labeled with radioactive nuclei or fluorescent dyes. Radioactive labels have very high sensitivity, but some of them have short half-lives and there is expense and waste disposal problems. Whereas fluorophores don't have this kind of problems and that's why they are the most common labels used for synthetic oligonucleotides. A label consist of three components: a signalling moiety, a spacer and a reactive group. The signalling moiety is the fluorescent part. The spacer separates the luminescent moiety from the oligo and can be used to change the hydrophobicity of the molecule. The reactive group helps the label to attach to an oligonucleotide. Some common oligonucleotides labelling reactions are listed in Appendix A.2 [8].

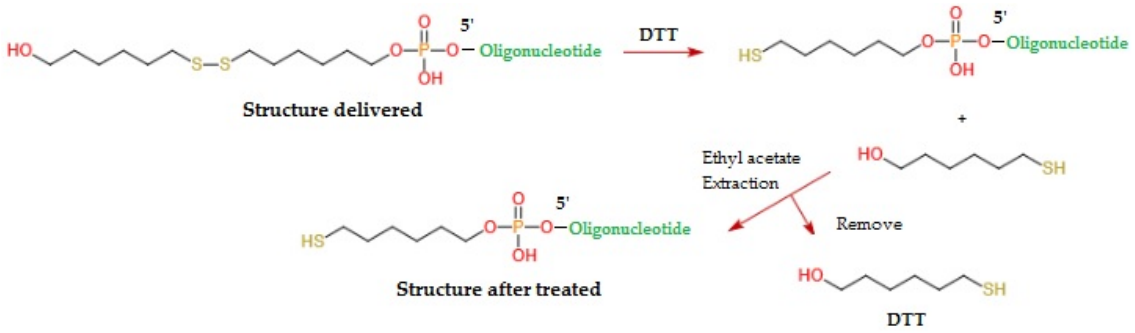

Figure 1.2: Treatment for thiol modified oligonucleotides [8].

Oligonucleotides can be thiol-modified, in which case they can be used for reaction with cysteines of proteins to make disulfide bonds and for binding to gold nanoparticles. Thiol-modified oligos can be synthesized by incorporating the thiol modification during solid-phase phosphoramidite oligonucleotide synthesis, at either the 5'-end or 3'-end of the oligo. Thiols are strongly nucleophilic and must be protected with the disulfide linkage to minimize the potential for oxidation, which results in oligo dimer formation. To use the free thiol (-SH) in applications, the disulfide linkage must be reduced with dithiothreitol (DTT). See Fig. 1.2 [8].

1.3 Electrical conductivity of DNA

Many mechanisms have been suggested of how the charge can transport in DNA. In this chapter some of these mechanisms are listed and introduced: electronic conduction along base pair sequences, ionic conduction associated with the counterions at the solvation shell surrounding the duplex, reorientation of the water dipoles around the duplex, and also phonons resulting from the structural fluctuations of the duplex. Experimentally, electronic and charge transport properties of DNA has been investigated by using scanning tunneling microscopy (STM), Raman spectroscopy, atomic force microscopy (AFM), and theoretically by using molecular dynamics (MD) and quantum mechanics (QM) simulations [9, 10].

Experimentally, it has been observed that charge transfer (CT) through the stacked aromatic base pairs of DNA is sensitive to the coupling of the donors and acceptors with the DNA. Also some of the electron orbitals belonging to the bases overlap quite well, which may help with electron transfer along the long axis of the DNA. It has been thought that these features of DNA CT may help to detect mutations, base lesions and protein binding. It may also enable charge transport over significant distances [11, 12, 13, 14].

Usually, the DNA is surrounded by positive "counterions", because the phos-

phate groups on the backbone are negative charged. It has been observed that it will generate current flow in the longitudinal direction in dsDNA, when protons are transported along the negatively charged phosphate backbone [13].

DFT calculations have showed that in watery medium, water orbitals increase the charge transport probability in DNA, which increase the conductivity of DNA. Results of the previous works on ssDNA and dsDNA have showed that the charge transfer likely happens through HOMO orbitals localized on the DNA bases, which mean that water molecules increase the charge transport probability because their π-orbitals contribute to the high-energy orbitals, including HOMO [12].

The charge transfer with phonons can be divided into oxidative hole transfer and reductive electron transfer processes. The hole transfer means that electron transfer in the opposite direction. The oxidative hole transfer is a HOMO-controlled process and the reductive electron transfer is LUMO-controlled (See Fig. 1.3). When DNA is photochemically or photophysically oxidized, it will create positively charged radical in DNA, which mean that an electron is transferred from the DNA. Respectively, the other process happens, when photoexcited electron of donor is injected into the DNA or transferred to the final electron acceptor. In order to avoid DNA damage, it's better to use the transport of excess electron rather than a hole during the sensing procedure, because hole transport can never occur without causing damage, whereas electron transport potentially can [15].

Gold nanoparticles (AuNPs) can be used for helping to detect small electricity variations. Different kind of DNA strands has different conductivity e.g. experimentally, it has been observed that, dsDNA has lower electrical resistance than ssDNA and when DNA monolayers are well-matched it exhibits a low resistance. So, it is possible to identify DNA with electrical current measurement [11, 16].

DNA is interesting molecule, which provides opportunity to build molecular devices, which can change their conductance as a function of pH. In addition, self-assembly feature of DNA makes possible to build new kind of two- and three-dimensional objects to electronic circuits [11, 15].

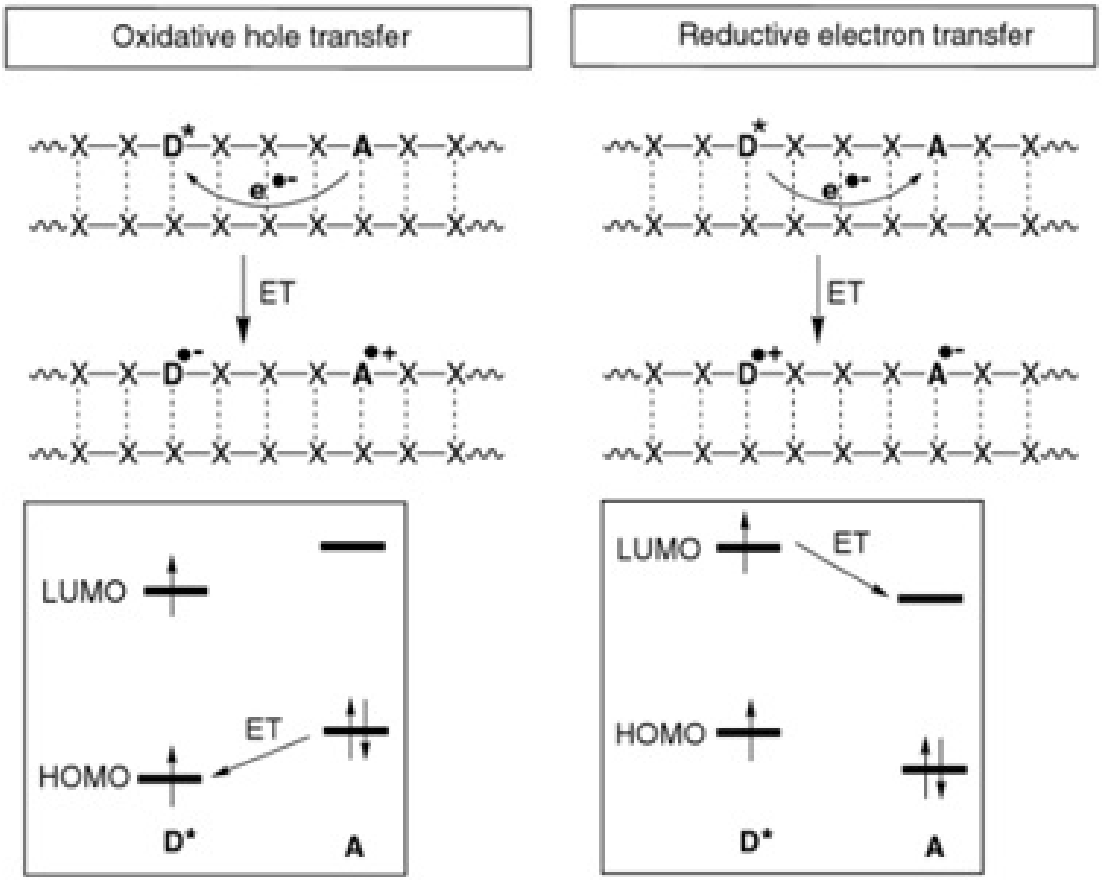

Figure 1.3: Comparison of photon induced oxidative hole transfer (HOMO control) and reductive electron transfer (LUMO control) in DNA (D = donor, A = acceptor, ET = electron transfer) [15].

Chapter 2

Dielectrophoresis

2.1 Fundamentals of dielectrophoresis

Dielectrophoresis (DEP) is a phenomenon in which a force is exerted on a polarizable particle, neutral or charged, by the non-uniform electric field. Polarizability determine how a material responds to a field (polarize), but it also determine the ability of a material to produce charge at interfaces. In DEP, alternating current (AC) fields of a very wide range of frequencies are used and to produce inhomogeneous field, sharp objects are used. Particle can feel positive- or negative-DEP by depending on a polarizability of the medium. If polarizability of particle is smaller than that of the medium, the particle feel negative DEP. Correspondingly, if polarizability of particle is greater than that of the medium, the particle feel positive DEP. See Fig. 2.1. The force on the particle will stay same, althoug the direction of the field changes every half cycle in the AC field. This is due to the fact that the induced charges will also change sides just like in Fig. 2.2 [17, 18, 19, 20].

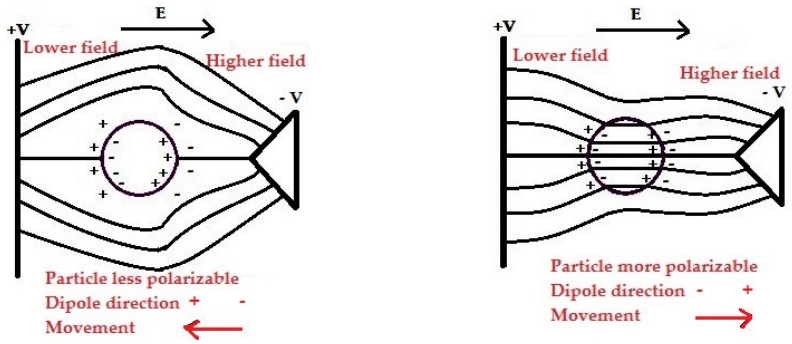

Figure 2.1: Negative and positive dielectrophoresis [18, 19].

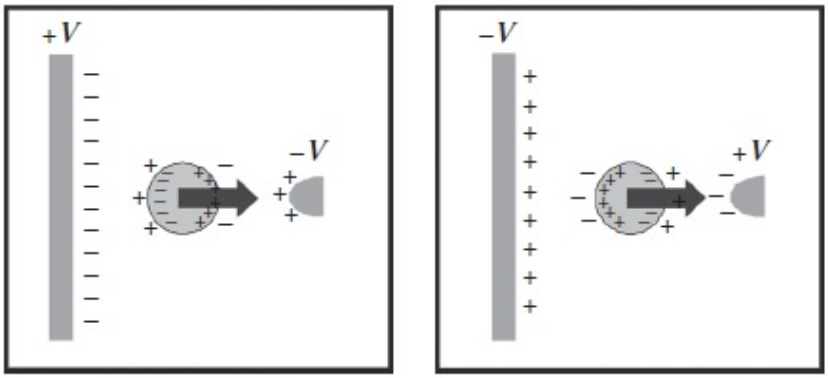

Figure 2.2: *When the electric field changes direction every half cycle in the AC case, the direction of the induced DEP force remains unchanged [18].*

2.2 Dielectrophoretic force and potential

2.2.1 Effective dipole and polarizability

A dielectric particle and its surrounding medium in the electric field $\vec{E}$ can be considered as an effective dipole with dipole moment $\vec{p}$ in such a way that

$$\vec{p} = \alpha \vec{E}, \tag{2.1}$$

where α is the effective polarizability [21]. The effective polarizability depends on the properties of the particle and the medium and on the frequency of the electric field according to equation

$$\alpha = 3V\epsilon_m Re\left\{K(\omega)\right\}, \tag{2.2}$$

where V descripes the volume of the particle, ϵ_m is the permittivity of the medium and $Re\left\{K(\omega)\right\}$ is real part of a Clausius-Mossotti factor [22]. This factor includes all the frequency dependence of the DEP force and is given by

$$K(\omega) = \frac{\tilde{\epsilon}_p - \tilde{\epsilon}_m}{\tilde{\epsilon}_p + 2\tilde{\epsilon}_m}, \tag{2.3}$$

where $\tilde{\epsilon}$ is the complex permittivity of the particle or medium. The complex permittivities of the particle and the medium can be related to the conductivity σ and angular frequency ω through the equations

$$\tilde{\epsilon}_p = \epsilon_p - i\frac{\sigma_p}{\omega} \tag{2.4}$$

$$\tilde{\epsilon}_m = \epsilon_m - i\frac{\sigma_m}{\omega}, \tag{2.5}$$

where i is the imaginary unit [17, 22].

2.2.2 DEP force

The dielectric force caused by an inhomogenous electric field can be written as

$$\vec{F}_{DEP} = (\vec{p}\cdot\vec{\nabla})\vec{E} = \frac{\alpha}{2}\vec{\nabla}(E^2). \tag{2.6}$$

For a periodically alternating electric field, $E(t)$ (period T), the time-averaged DEP-force can be written as

$$\vec{F}_{DEP,t} = \frac{1}{T}\int_0^T \frac{\alpha}{2}\vec{\nabla}\left|E(t)\right|^2 dt = \frac{\alpha}{2}\vec{\nabla}\left\{\int_0^T \left|E(t)\right|^2 dt\right\} = \frac{\alpha}{2}\vec{\nabla}(E_{rms}^2), \tag{2.7}$$

where E_{rms} is a root mean square value of an electric field [17, 22]. For a sphere with radius r_p, the time-averaged DEP-force is

$$\vec{F}_{sphere,t} = 2\pi\epsilon_m r_p^3 Re\left\{K(\omega)\right\}\vec{\nabla}(E_{rms}^2). \tag{2.8}$$

2.2.3 Trapping by DEP and the Brownian motion

Small particles can be trapped, when the obtained DEP force exceeds a Brownian motion. The Brownian motion is a random force, which is caused by the thermal motion of particles in a fluid. The maximun value of the force for a spherical particle is approximately

$$F_B = \frac{k_B T}{\sqrt[3]{V}}, \tag{2.9}$$

where k_B is Boltzmann's constant, T the temperature and V the volume of the particle [18, 22]. A volume of thiol-modified and Cy3-dye labeled oligonucleotide is approximately 14.3 nm^3. So, the Brownian motion for oligo is approximately $1.67\cdot10^{-12}$ N at room temperature (300 K). The polarizability for a 40 nt ssDNA is $\alpha \approx 2\times10^{-33}$ Fm^2 [23]. In this case the gradient of the electric field square should reach values of the order of 10^{21} V^2/m^3 to make Brownian motion negligible.

2.2.4 DEP potential

Another way to describe the trapping of particles is based on a DEP potential, which is a potential energy generated by DEP trapping. DEP potential for a polarizable particle in the electric field is

$$U_{DEP} = -\frac{1}{2}\alpha E^2, \tag{2.10}$$

where the effective polarizability α depends on the frequency ω of the applied signal and on the properties of the particle [23, 24]. Combining the DEP potential with the thermal energy of a particle, the total potential energy get shape:

$$U_{total} = U_{thermal} + U_{DEP} = \frac{3}{2}k_B T - \frac{1}{2}\alpha E^2. \tag{2.11}$$

Equation shows, that the total potential energy achieve it's minimum value at the point of the highest electric field. The particle will be trapped, when the DEP potential U_{DEP} is higher than thermal energy $U_{thermal}$ [23, 24].

2.3 Dielectrophoretic trapping of nanoscale objects

DEP has been widely used for manipulation, separation and trapping of various objects (biomolecules, latex beads, viruses, etc.) in the micro- and nanoscale. DEP trapping requires high electric field areas, where the value of DEP potential is higher than the thermal energy of object. Usually these kinds of areas are at electrode edges [23, 24, 25].

DEP force depends of the polarizability of the object. For small molecules, the Brownian motion is large and the polarization is small, which lead to that the effect of the DEP force is small (See Equations 2.6 and 2.9). So, to get required DEP force for winning the Brownian motion of small particles, the very high electric fields are needed. In DEP trapping process, a frequency dependence occurs thereby, that more DNA is trapped with lower frequencies than higher, but on the other hand, with higher frequencies the DNA is better localized in the desired point [23, 24, 25].

In Part II of this thesis the DEP trapping of 40 nt long oligos to triangular AuNPs is discussed. These oligos were thiol-modified and dye-labeled. Whereas, the triangular AuNPs were 20 nm thick and side length was 1 µm. Details of sample fabrication, DEP trapping methods and results are showed in Part II. In the next chapter is reviewed theoretically fluid dynamics in nanoelectrode system: how theoretically different flows are born and how they appear in DEP.

Chapter 3

Fluid dynamics in nanoelectrode system

3.1 Electrothermal fluid flow

In non-uniform electric field, the temperature varies by regions creating spatial variations in conductivity, permittivity, and viscosity. These variations cause different flows in the system. One of these flows, is electrothermal flow, which results when electric field-induced Joule heating creates spatial variation in electrical properties of fluid resulting in localized bound charge densities that are then subject to significant Coulomb forces. This flow drives particles in closer to the corner where they are subjected to significantly higher DEP forces, however this same flow also drives particles farther from these high DEP force regions. This driving away flow is stronger and that's why electrothermal flow drives particles farther from high DEP force regions [26, 27, 28].

The electrostatic force density acting on an aqueous solution in the presence of an electric field is

$$F_{ET} = \rho_e E - \frac{1}{2} |E|^2 \nabla \epsilon_m, \tag{3.1}$$

where ρ_e is local charge density, E the electric field and ϵ_m electrical permittivity. Because ρ_e and E are oscillating at a frequency ω, the volume force is composed of a steady term and an oscillating force, of frequency 2ω. The time-averaged form of this force is

$$\langle F_{ET} \rangle = \frac{1}{2} Re(\rho_e E^*) - \frac{1}{4} E \cdot E^* \nabla \epsilon_m, \tag{3.2}$$

where * indicates complex conjugate [26, 27, 28].

3.1.1 Joule heating

Joule heating is caused by interactions between the moving particles (form the current) and the ions of the conductor. When charged particles collide with these ions, they give up some of their kinetic energy to ions. This increase the vibrational energy of the ions, which is manifested as a rise in the temperature of the conductor. If the surrounding medium is thermally conductive, the heat will transfer to it. Joule heating corresponds to the electrical energy generated per unit volume

$$Q = J \cdot E = \sigma_m E \cdot E = \sigma_m E^2, \tag{3.3}$$

where J is the electric current and σ_m the electrical conductivity of the fluid [26, 27].

3.1.2 Convection flow

In convection flow, the heat from the heat source start to move towards colder area. This warm flow push out the cold area on its way, which gets cold region to move towards the heat source. This will give birth to the flow, where warm area moves to colder area and colder area moves to warm area. In DEP, this phenomenon push molecules away from the electrodes, because these molecules act like heat source [26, 27].

The steady time-averaged temperature field, T, in the fluid is governed by the following energy equation:

$$\rho_m C_p \frac{\partial T}{\partial t} - k\nabla^2 T = Q - \rho_m C_p u \cdot \nabla T, \tag{3.4}$$

where ρ_m is fluid density, C_p the heat capacity in constant pressure, u the fluid velocity and k is the thermal conductivity of the fluid [26, 27]. The time dependent term on the left-hand side of the equation can be shown to be negligible. So, starting from the heat conduction equation

$$\frac{\partial T}{\partial t} = \frac{k}{\rho_m C_p}\nabla^2 T, \tag{3.5}$$

some approximations can be done: $\partial T/\partial t \approx \Delta T/\Delta t$ and $\nabla^2 T \approx \Delta T/l^2$, where l is the gap between the electrodes. Hence, the diffusion time across the gap is

$$t_{diff} = \frac{\rho_m C_p l^2}{k}. \tag{3.6}$$

The thermal properties of the fluid can be assumed to be same as for water ($\rho_m = 1000$ kg/m^3, $C_p = 4200$ J/(kg·K) and $k = 0.6$ W/(m·K)). If the gap between the electrodes is 10 µm (20 µm), then the diffusion time is 0.7 ms (2.8 ms).

If AC field have an angular frequency $\omega = 2\pi f$, where f is frequency, the total temperature T is a sum of time-averaged term T_0 and $\Delta T(t)$ which depends on 2ω. Thus, the differential temperature $\Delta T/T$ can be approximated from Eqs. (3.5) and (3.6) to be

$$\frac{\Delta T}{T} \approx \frac{1}{2\omega t_{diff}}. \tag{3.7}$$

The differential temperature is negligibly small for fields with high frequency, and thus only the time-averaged temperature has to be considered. This affect Eq. (3.4) so that the first term on the left-hand side can be ignored and the Joule heating term given by Eq. (3.3) must be time-averaged. If the solution for the electric potential represents the peak value, then the time-averaged value is obtained by dividing the peak value by $\sqrt{2}$. From this it follows that the time-average of the Joule heating term is Eq. (3.3) divided by two. With this approximation, the Eq. (3.4) get form

$$\rho_m C_p u \nabla T = k\nabla^2 T + \frac{1}{2}\sigma_m E^2. \tag{3.8}$$

The second terms on the left-hand and right-hand sides of Eq. (3.4) describe the diffusion and convection of heat, respectively. By approximating that the effect of convection is negligible compared to diffusion, the convection term can be ignored from Eq. (3.4) as shown below

$$\left| \frac{\rho_m C_p u \cdot \nabla T}{k\nabla^2 T} \right| \approx \frac{\rho_m C_p u l}{k} << 1. \tag{3.9}$$

After all these approximations Eq. (3.4) gets the form

$$k\nabla^2 T + \frac{1}{2}\sigma_m E^2 = 0, \tag{3.10}$$

Substituting the approximations $\nabla^2 T \approx \Delta T/l^2$ and $E = V/l$ into Eq. (3.10) gives expression for the temperature rise:

$$\Delta T \approx \frac{\sigma_m V_{rms}^2}{2k} = \frac{\sigma_m (0.354 \cdot V_{pp})^2}{2k}, \tag{3.11}$$

where V_{rms} is root mean square voltage and V_{pp} peak-to-peak (pp) voltage of applied AC signal. The conductivity for high quality deionized water is about 5.5 µS/m. So, if the pp voltage between electrodes is 1 V (40 V) and the thermal conductivity of the fluid 0.6 W/(m·K), the temperature rise is approximately 0.6 µK (0.9 mK). The conductivity for drinking water varies from 5 to 50 mS/m. The minimum temperature rise for drinking water with 1 V (40 V) is 0.5 mK (0.8 K) and maximum is 5.2 mK (8.4 K) [26, 29, 30].

3.2 AC electro-osmotic flow

3.2.1 Electrical double layer

When electrolyte surrounds charged particles, it will form thin interface, called electrical double layer (EDL), between the surface of particle and the electrolyte surrounding particle. The first layer is surface of the particle and the second layer consist of Stern layer (fluid near the surface is immobile) and diffuse layer. For DNA, this second layer is positively charged and it consists of ions (counterions), which are from solution. See Fig. 3.1. AC electric field causes counterion polarization. Since there is Coulombic attraction between the charged particle and the counterion layer, the counterions attempt to pull the charged particle along with them as they follow the electric field [20].

The thickness of the EDL is often estimated by the Debye length κ^{-1} which is

$$\kappa^{-1} = \sqrt{\frac{\epsilon k_B T}{e^2 \sum_j c_j^\infty z_j^2}}, \tag{3.12}$$

where ϵ is the permittivity of the electrolyte, k_B the Boltzmann's constant, T the temperature, e the elementary charge, c_j^∞ the concentration of the ions of type j in the bulk electrolyte and z_j the charge number of the ion of type j [31].

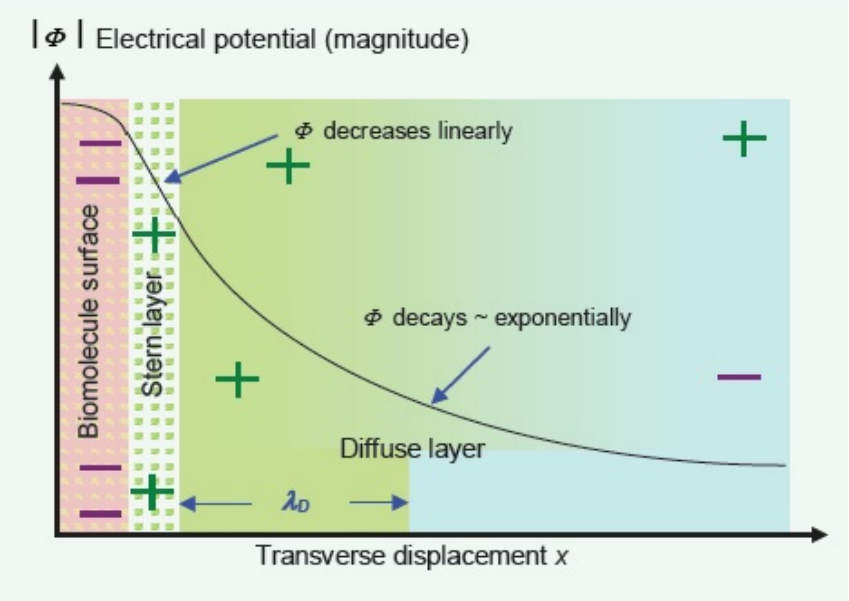

Figure 3.1: Stern model of the electrical double layer [20].

3.2.2 Electric field

AC electro-osmotic (ACEO) fluid flow is generated by the interaction of the tangential component of the nonuniform electric field with the induced charge in the EDL on the electrode surfaces. Previous experimental studies has demonstrate that the fluid is driven at the surface of the electrodes. In the nonuniform AC field, the fluid moves within the high field strength regions on the edges of the electrodes with the highest velocities found at the edge. This flow depends on the frequency and amplitude of the applied signal and on the electrolyte conductivity as it can be seen from the Eq. 3.13 [32, 33].

The simplified ACEO velocity expression for the system with two wide electrodes with an infinitesimal gap in between is

$$v_{ACEO} = \left(\frac{\epsilon V_0^2 f_{non}^2}{8\eta x (1 + f_{non}^2)^2} \right) \tag{3.13}$$

$$f_{non} = \frac{1}{2} \pi \kappa x \left(\frac{\epsilon_m}{\sigma_m} \right) \omega, \tag{3.14}$$

where V_0 is the applied electric potential, f_{non} is a non-dimensional frequency defined as above, η is the dynamic viscosity, x is the horizontal location starting from the center of the gap between the electrodes, and κ is the reciprocal of the Debye length [33].

The Fig. 3.2 shows the mechanism of ACEO in the system with two electrodes separated by small gap. The electric field's tangential component E_x produce a force F_c, which drags fluid away from the center of the gap [32].

3.3 Natural convection

The process, where the flow arises "naturally" from the effect of a density difference, resulting from a temperature or concentration difference, is termed natural convection. In this process, the density difference gives rise to buoyancy forces due to which the flow is generated [34].

Natural convection is widely used for cooling electronic equipment, because its simplicity of design, low operating costs due to no extra power requirements, minimum maintenance, absence of noise due to no additional moving part, and very high reliability. Previously, in the convection low chapter, temperature rise for water medium was estimated. The effect of the natural convection in nanoelectrode systems can be ignored, because the temperature rise is very small [35].

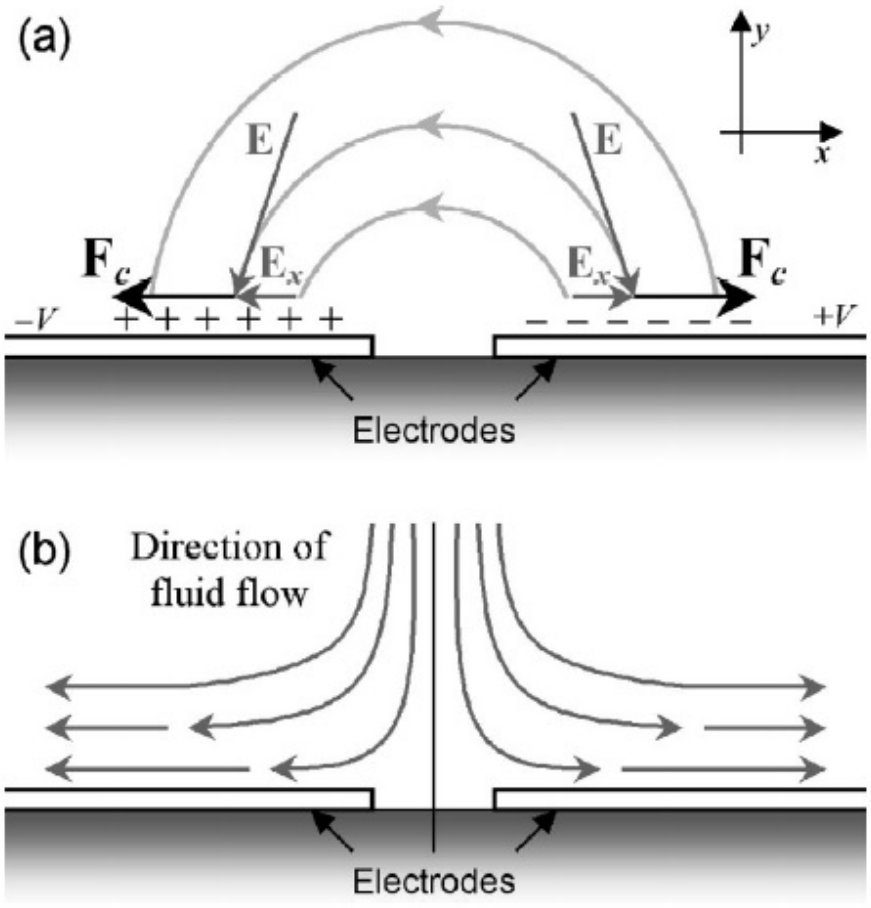

Figure 3.2: Principle of the ACEO fluid flow [32].

Part II

Results and Analysis

Chapter 4

Experimental methods

4.1 Sample preparation

Thiol-modified oligonucleotides were purchaced from Integrated DNA Technologiest (IDT) company, but the electrodes and triangles systems (Fig.4.1) were prepared in here.

4.1.1 Window preparation

Windows were fabricated by using photolithography, Si_3N_4 etching with reactive ion etcher (RIE) and wet etching (34-% KOH solution). Windows were 1 µm thick and side length varied from 70 µm to 470 µm. After window preparation, electrodes and triangles were fabricated on top of the Si_3N_4-window.

4.1.2 Electrode preparation

Electrodes were fabricated by using standard electron-beam lithography method and evaporation of metal (5 nm of Ti followed by 20 nm of Au) in an ultrahigh vacuum (UHV). Before the DEP trapping, residues from the lift-off were removed by an oxygen plasma cleaning in a reactive ion etcher.

A more detailed description of building electrodes and triangles systems can be found from Ref.[36].

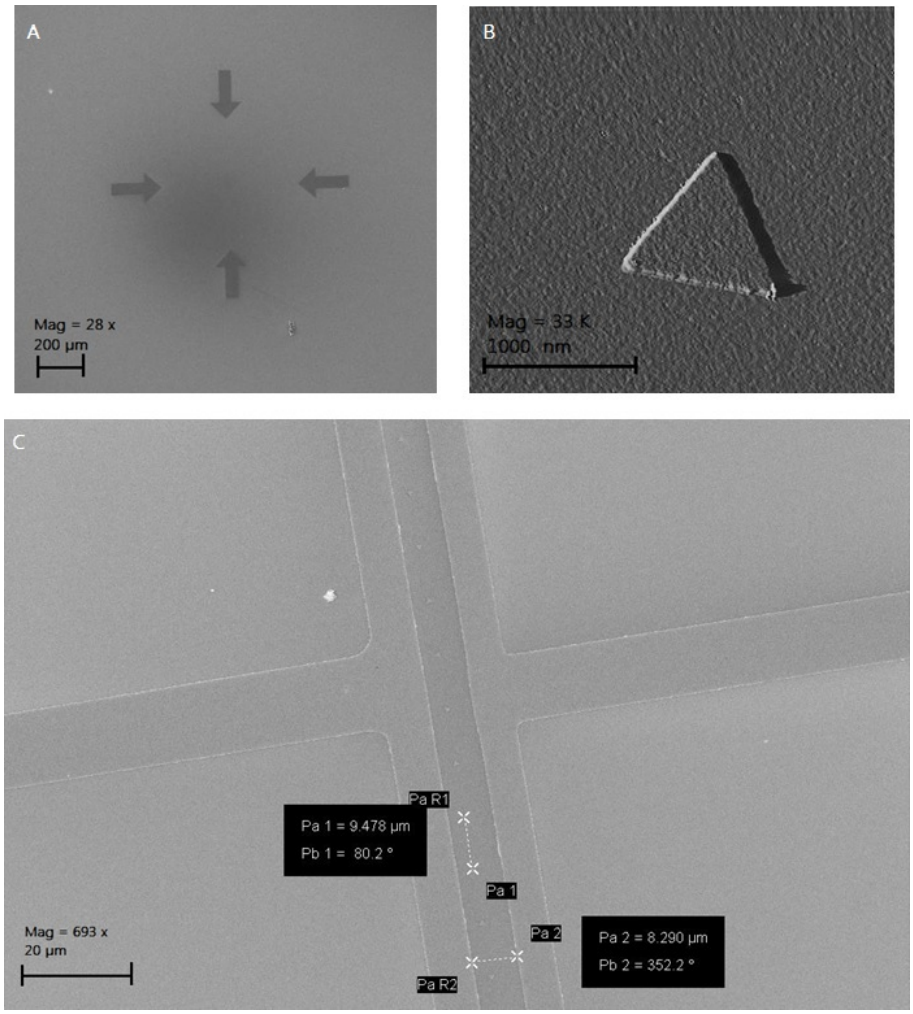

Figure 4.1: Figure A is a SEM-image of a system with 4 marker arrows. There is 100 triangles in the middle of this system. Figure B is a closer image of one triangle. Side length of the triangle is about 1 µm. (This image has been taken with AFM.) There is 19 triangles between two electrodes in figure C. The gap between electrodes is about 10 µm.

4.2 Dielectrophoretic trapping

The DEP trapping was done in different concentrations of Cy3-marked oligos (also Cy5 was tested) diluted in deionized water. Some DTT was added into the DI-water to reduce the thiol-thiol bondings. Cy3/Cy5-sample, DTT and DI-water was mixed and stored in the eppendorf tubes.

Oligos were 40 nt long and their sequences were 5'-$(CT)_{16}$GATGGCTT-3'-Cy3 and 5'-$(CT)_{16}$GATGGCTT-3'-Cy5. The strands were thiol-modified ($C_6H_{12}SH$) in the 5'-end (See Figure A.3).

4.2.1 Triangles with arrows

The first system, what was used for trapping included 4 marker arrows and 100 triangles. A cuvette was used as a trapping container. The chip was set on the cuvette's sample holder (See Figure 4.2). Then the cuvette was filled with Cy3/Cy5-dilution and the system was connected to AC-circuit. After trapping, the chip was cleaned with DI-water, dried with nitrogen gas and imaged with Olympus FluoView FV1000 Confocal Microscope. Dilutions and trapping parameters are tabulated in Table B.1 in appendix B.

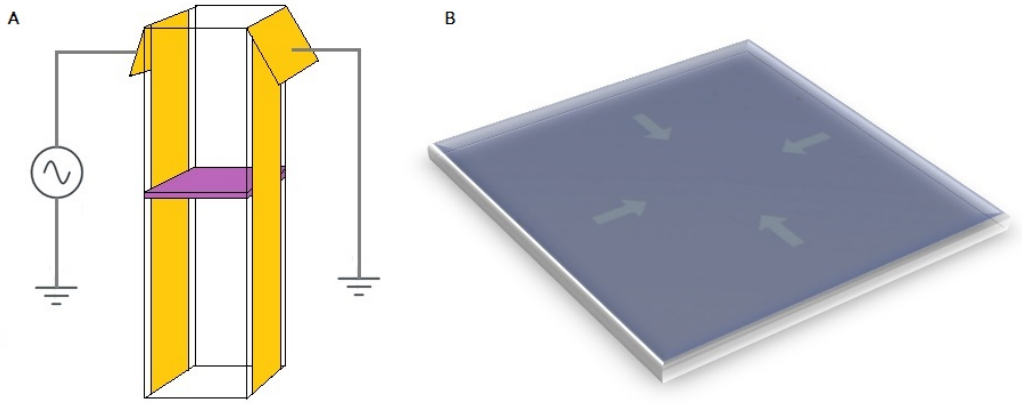

Figure 4.2: A schematic view of the experimental set-up used in the first oligo DEP experiments. The chip is inside the cuvette, which has two copper electrodes. In the middle of the chip, there is triangles with arrows structure. In this structure, there is 100 triangles and four marker arrows.

4.2.2 Triangles with electrodes

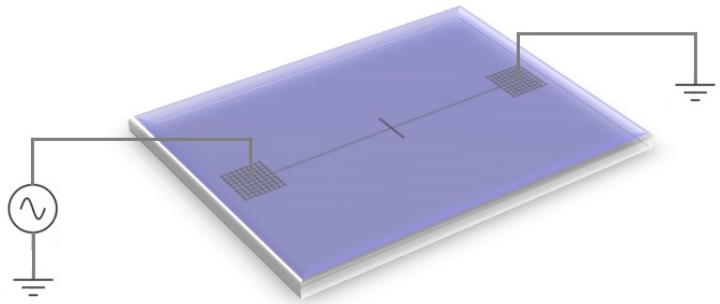

Figure 4.3: A schematic view of the experimental set-up used in the second oligo DEP experiments. Electrodes are connected to AC-circuit with two sharp probes (like in figure). The chip is covered with oligo-dilution and the trapping experiment is done inside a protected box.

The second system included two gold electrodes and 19 gold triangles (see the design from fig. 4.1 c). The system was connected to AC-circuit with two sharp probes and oligo-dilution was added on the chip (See Figure 4.3). After trapping, the chip was treated like in the first case. Dilutions and trapping parameters are tabulated in Table B.2.

4.2.3 Triangles with electrodes and window

After seeing that the second system didn't yet work like was wanted, the system were changed little bit. To reduce silicon's effect on the electric field it was etched away under the electrodes leaving only a thin Si_3N_4 membrane window as a substrate. Otherwise the trapping was performed in the same manner. Dilutions and trapping parameters are tabulated in Table B.3.

In the previous systems very little oligos were seen, and those seemed to settle down randomly everywhere. To ensure that the oligos move with the electric field, it was decided to do the trapping experiment and imaging at the same time (live-trapping). For this purpose system like in Figure 4.4 was built. After adding the oligo-dilution, the chip was covered with cover glass and the trapping experiment was done under a confocal microscope. Dilutions and trapping parameters are tabulated in Table B.4.

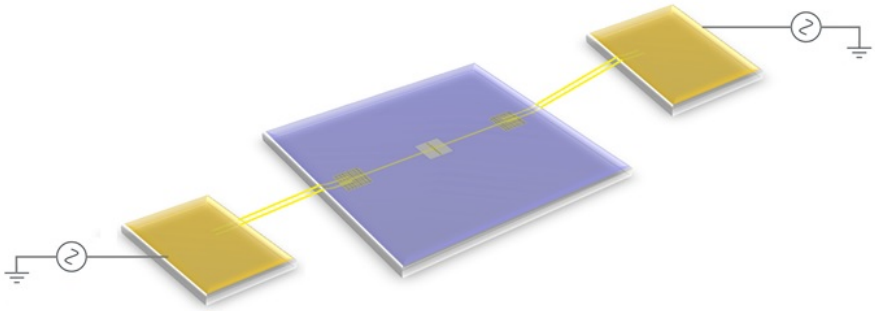

Figure 4.4: A schematic view of the experimental set-up used in the oligo live-DEP experiments. In the middle, there is the electrodes with triangles in between and under it, there is a Si_3N_4-window. The whole system is laying on a microscope slide glass.

4.2.4 Trapping results

The gathering of the oligos to the triangles and electrodes was studied after trapping or in situ during the trapping, i.e. live DEP, by confocal microscope (Olympus FluoView FV1000, 10 - 100 x dry/oil objectives, lasers 543 nm and 633 nm were used to excite Cy3 and Cy5 dyes).

In our trapping system we first used oligos which were Cy5-labeled, but the fluorescent was so weak that we had to change to Cy3-labeled oligos. In Fig. 4.5, we can see that triangles were surrounded by a strange circles when Cy5-dye were used. We don't know is there oligos in these circles, because the fluorescent signal was so weak. When we changed fluorescent dye, we didn't see anymore these circles, but we saw better where the oligos were (See Fig. 4.5).

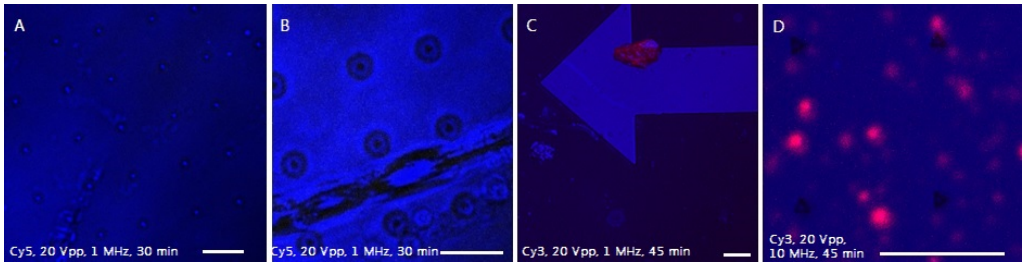

Figure 4.5: Confocal microscope images of triangles with arrows system. White scale par in each images is about 10 µm.

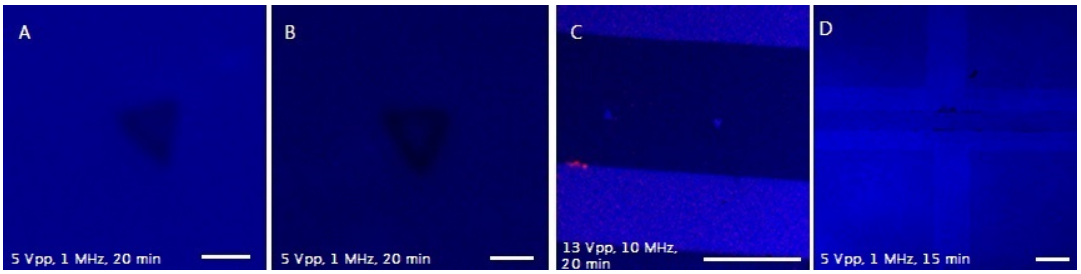

Figure 4.6: Confocal microscope images of triangles with in the electrodes system. White scale par in images A and B is about 1 µm and in images C and D about 10 µm. Image C is from triangles with electrodes and window system. It is taken from area, which is not on the window.

In this first system, oligos were trapped randomly everywhere and only in couple of triangles there were oligo lumps seen in corners. We thought that by this system, we don't get DEP force large enough that would pull the oligos to the corners of the triangles. So, we decided to built a new system, where the electrodes were near to the triangles.

In the second system, oligos didn't trap to the corners of the triangles, but they trapped to the electrodes. There were more oligos on the source electrode than on the ground electrode, because the silicon substrate is capacitively well connected to ground and that affects that DEP is more powerful at the source electrode than at ground electrode (See Fig. 4.6). In this system we only see few oligos, because the concentration of the oligos were so small.

In order to ensure that silicon don't induce anymore problem, it was decided that the system should be built on the silicon nitride window, which does not affect same kind of problem as silicon. So, in this third system triangles and electrodes are laying on the window. This time we also used much more higher voltages to get high DEP force.

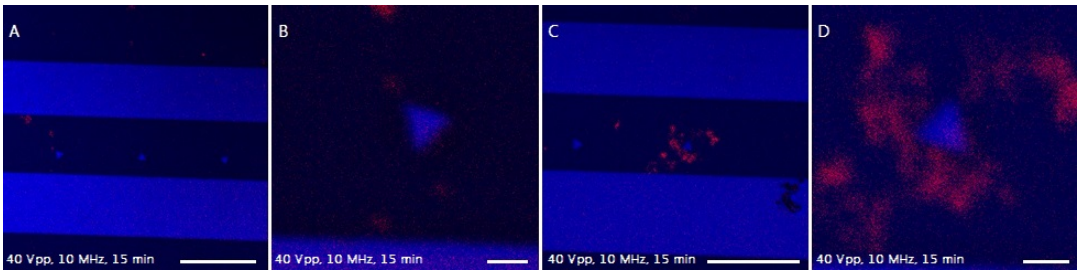

Figure 4.7: Confocal microscope images of triangles with electrodes and window system. Triangle is surrounded by oligos. White scale par in images A and C is about 10 µm and in images C and D it is about 1 µm.

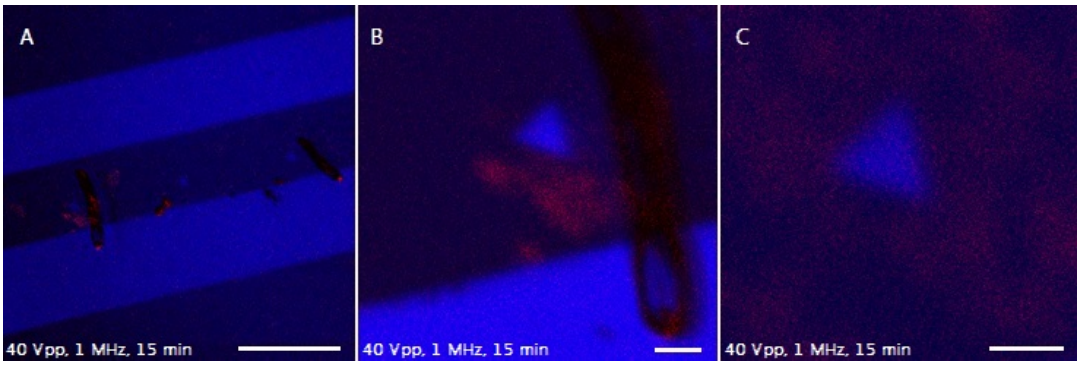

Figure 4.8: Confocal microscope images of triangles with electrodes and window system. White scale par in image A is about 10 µm and in images B and C it is about 1 µm. Aggregated oligos were worm like and only little fluoresce was detected.

Window and higher voltages really helped the system, because now there were more oligos near triangles and in couple of cases one or two triangles were surrounded by oligos (See Fig. 4.7). But we still didn't see any oligos on the corners and we saw only few oligos. Also the fluorescence disappeared really fast. Then second problem was that, if the oligo sample were too long time in the fridge and not in the freezer, the oligos start to aggregate as shown in Fig. 4.8.

We tested for couple samples to dilute oligos to buffer instead of pure DI-water, but in this case we hardly see any oligos with confocal microscope. So, the water is still better for our system. When we didn't dry the sample after trapping, but directly did imaging, we saw more oligos and actually we also saw little movement of oligos there, because those oligos which were still not trapped move with water evaporation flow, just like in Fig. 4.9.

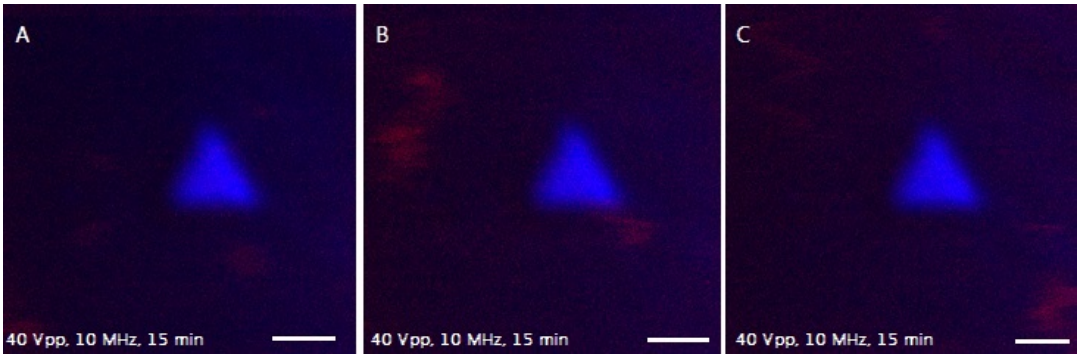

Figure 4.9: Confocal microscope image-series of a triangle with electrodes and window system. System is still wet and oligos move with water evaporation flow. White scale par in all images is about 1 µm.

In the live-DEP, we did trapping and imaging at the same time. In live-DEP experiments a 60 x water objective was used for imaging, because the system was now in water environment. When system is still wet, oligos can also move with water evaporation flow (See figure B.1 in Appendix B).

When the oligos were aggregated, we saw big oligo lumps which move with electric field and trapped on the electrodes (See image series 4.10). When we made new oligo dilution, we saw only much more smaller oligo dots which move between the electrodes.

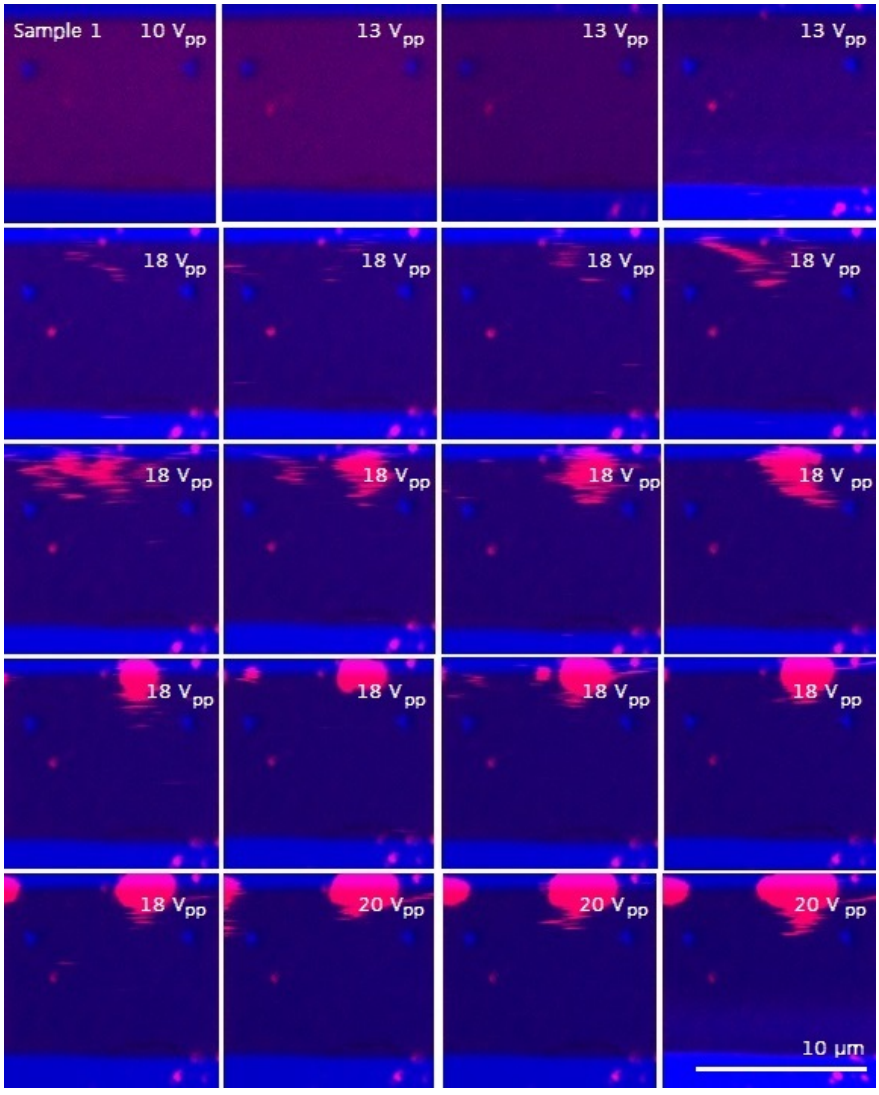

Figure 4.10: Live-DEP image series of system, where oligos are aggregated. The trapping voltage was increased in steps as shown on the corners of the images.

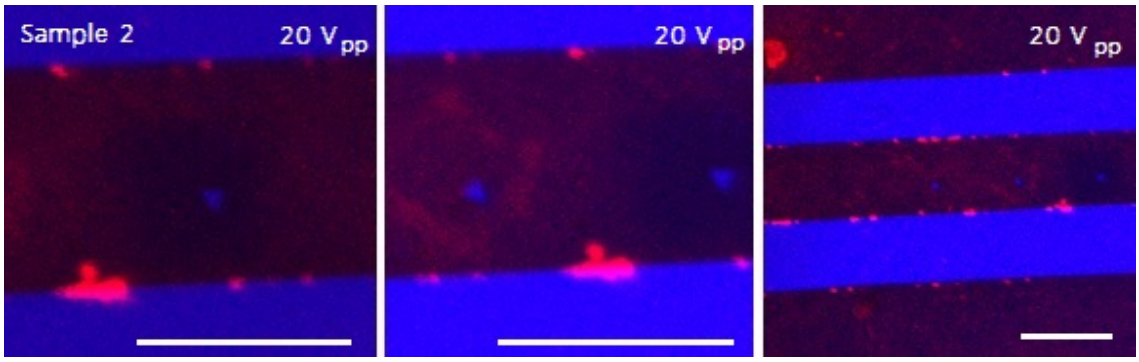

Figure 4.11: Live-DEP and loss of fluorescence. White scale par in each images is about 10 µm.

In one sample, we had a little too much exposured electrodes with smaller gap in the middle of the structure and also these electrodes had small scratches. During live-DEP, when voltage was turned on, the system initially operated in the normal way, but when accidentally the square wave (voltage is about 50 V_{pp}) turned on, then started to happen. The electrodes quickly started to crack from these scratch and these scratch started to gather oligos. View figure series from Appendix B.2.

In the live-DEP imaging the same problem as in the dry imaging system appeared; if you imaged same area for a long time, the fluorescence disappeared. This can be seen very well in the Fig. 4.11, in which the fluorescence does not appear in the surroundings of the triangle, which has been closely imaged for a very long time. Next to this triangle is a triangle, which is not imaged near for long time and there is lots of fluorescence visible close to the triangle. The figure also shows that the large lumps of oligos trapped to the electrodes and the individual smaller oligos remain near the triangle.

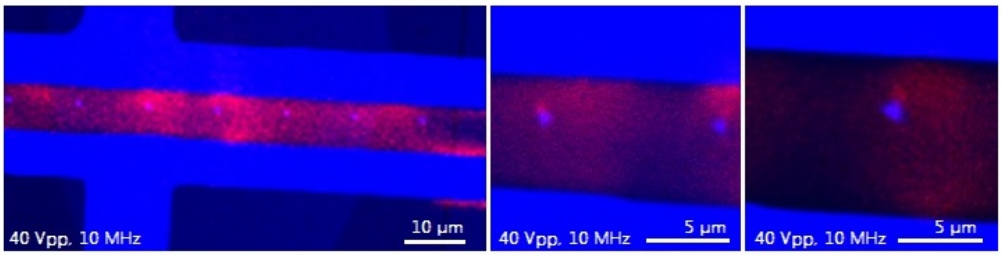

Figure 4.12: Triangles are attracting oligos. When oligos are not on the window, they will be trapped to the electrodes and when they are on the window, they are floating around the triangles and sometimes some of them goes to the corner of the triangle.

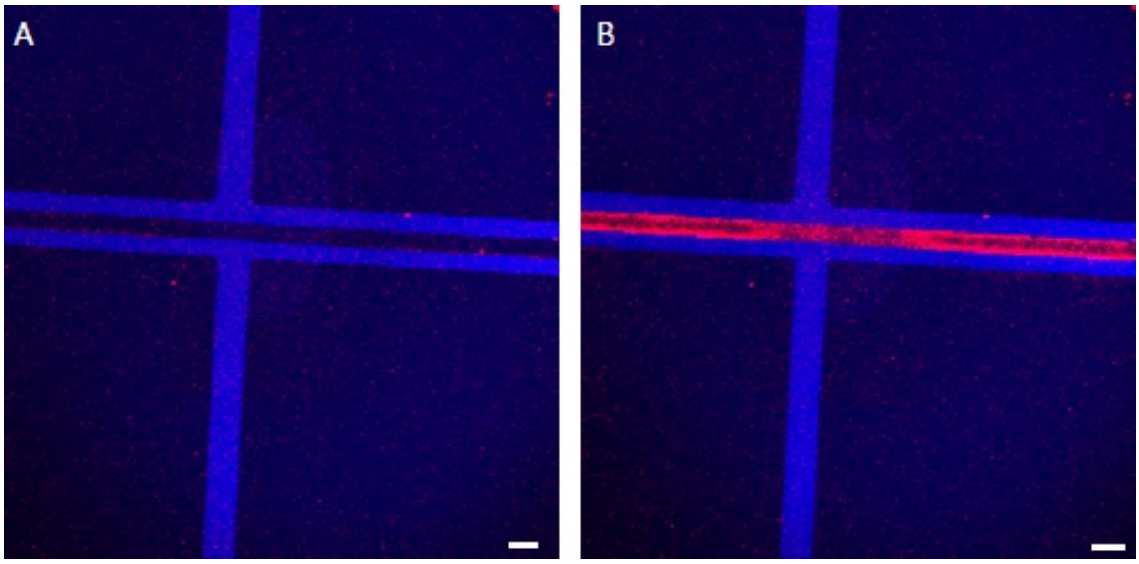

Figure 4.13: What happen to fluorescence, when system is connected to high voltage (over 35 V_{pp}). When voltages is OFF (image A) and ON (image B). White scale par is about 10 µm.

During the last live-DEP imaging, we got a clear proof that the triangles are attracting oligos. Oligos formed a "cloud" around the triangle and also in a few cases, there was clearly observed that oligos were trapped to the corners of the triangles. See Fig. 4.12. Also from the same figure, it can be seen what is the difference when the system is on the window and when it is not.

During the live-DEP it was also observed that when you turn off voltage, oligos disappeared and when you turn on, you can again see the oligos. So, when the high voltage is ON, with high speed it will trap lot of oligos, which increase the total fluorescent. When voltage is switched off, the oligos are driven elsewhere and the total fluorescent decrease. So, the oligos didn't attach to gold with thiol-group. See Fig. 4.13.

Chapter 5

Electric field and DEP force simulations

To obtain some theoretical basis for trapping, the electrode system was modeled by using COMSOL Multiphysics software (version 4.3 and 4.4). In the modeling different kind of electrodes were used. Wide, narrow, thin and finger-likes electrodes were tested. For all systems: the electric field and DEP force were simulated by using finite element method (FEM). DEP force's dependency on orientation of triangles was also tested.

5.1 Building the model

All models were built in 3D and chosen application mode was Electrostatic (es) from AC/DC module and study type was Stationary. With this model type we can model DC voltage system. However, our experimental system works with AC voltages, but we can use DC model to describe our system, because DC voltage values correspond to RMS values in the case of AC signals. So, the peak-to-peak values need to be changed to rms values.

5.1.1 Triangle

Triangle was built by first drawing 2D polygon with work plane and then doing extrude to get 3D structure (Fig.5.1). Orientation of triangle can be changed by adding rotate component to plane geometry.

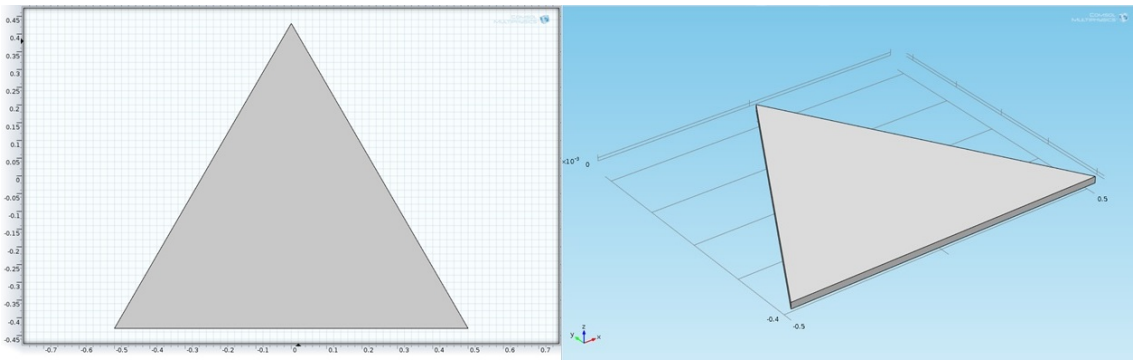

Figure 5.1: Equilateral triangle with side length of 1 µm and 20 nm thickness.

5.1.2 Cube

All systems were built in different volumes of cubes depending how large gap we wanted between the electrodes and what kind of electrodes were used. Model 1.1. is used for an example.

Cube with a side length of 11 µm have been built and two 0.5 µm thick layers has been added on two opposite edges/sites. These layers will be working as electrodes. So, the gap between two electrodes is 10 µm (Fig.5.2).

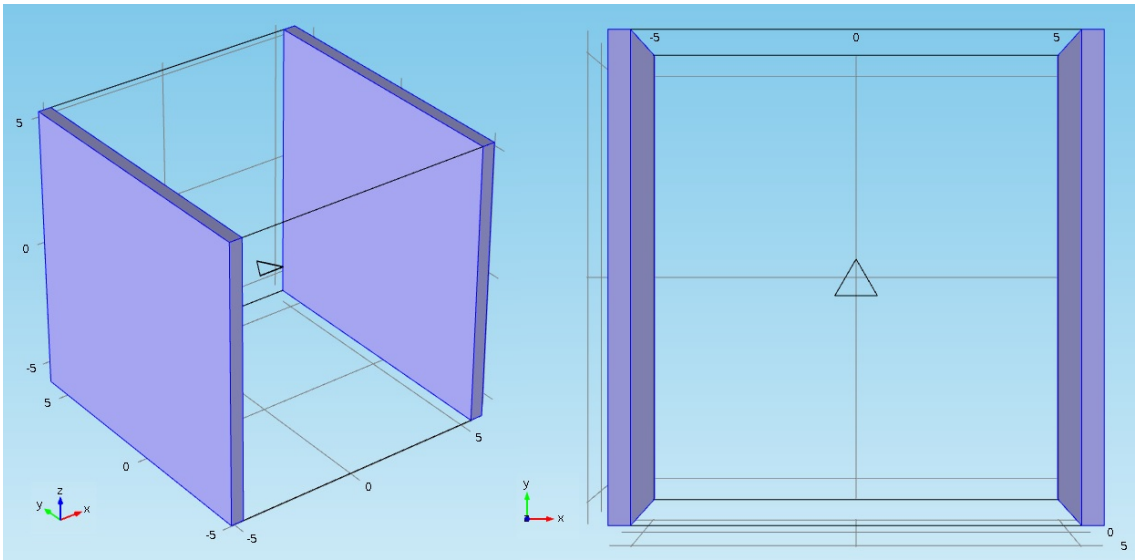

Figure 5.2: Model 1.1. has 10 µm gap between two electrodes, which cover hole walls of the simulation cube.

5.1.3 Materials, Electrostatics and Mesh

All domains were built in water (relative permittivity $\epsilon = 80$) in models 1, 2 and 3. Model 4.1 includes also SiO_2 -layer ($\epsilon = 4.2$) and Si -layer ($\epsilon = 11.7$) and models 4.2 and 4.3 have Si_3N_4 -layer ($\epsilon = 9.7$). We also test one system, where we needed air layer ($\epsilon = 1$).

Electrodes were chosen to be infinite elements with equipotential surface as a edge, floating potential was added to triangle, right electrode was chosen to be ground and left one was chosen to be electric potential source in Electrostatics section. Electric potential is now DC value, which corresponds RMS value in the case of AC.

In Mesh section, electrodes were meshed with swept mesh; medium and triangle with free tetrahedral mesh. Equipotential surface can be get by using swept mesh (Fig.5.3).

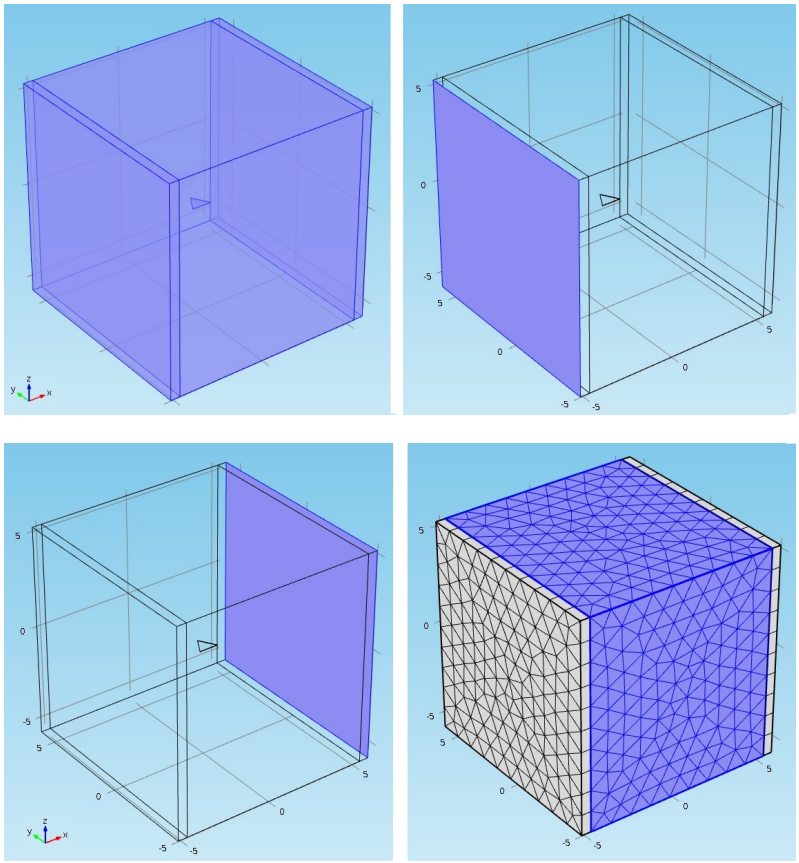

Figure 5.3: All domains in water, left electrode source, right one ground and mesh structure.

5.2 Results

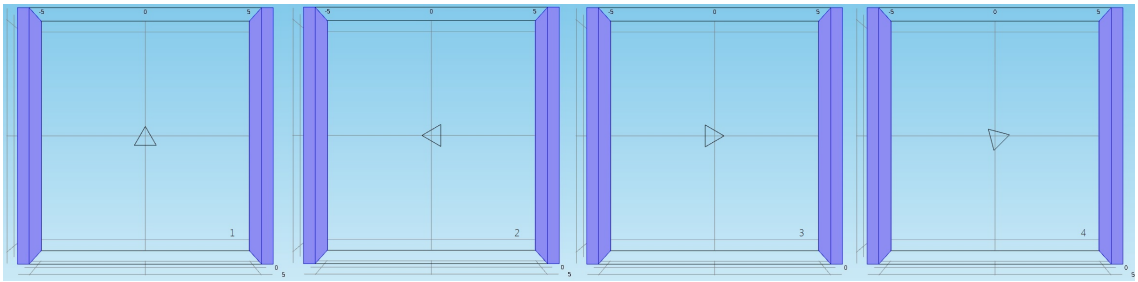

Figure 5.4: Four different orientation for triangle. Left electrode is always voltage source and right electrode is grounded.

The values and images were simulated for the electric field, the DEP force, i.e., the gradient of the square of the electric field (SI-units: V^2/m^3) and in addition to the logarithm of the gradient of the square of the electric field. The last of these simulations show the best places where our oligos should be trapped.

Simulations were carried out with six different voltage value. In addition, for each model the minimum voltage to obtain the necessary DEP force in order to trap oligos were searched.

For symmetry reasons, the triangle was modeled by using only four different orientations (Fig.5.4). All these orientations were simulated only for model 1.1. The rest of the simulations were carried out only for one orientation, because the magnitude of the DEP force appeared to depend only slightly of the orientation of the triangle (See Appendix: C.1). The orientation number 4 was chosen from all these orientations, because if we would have free triangles in solution, the majority of them would likely be oriented somewhat like this.

5.2.1 Model 1

Triangle is floating in water medium and electrodes cover two opposite walls of the simulation cube in model 1. In model 1.1 the gap between electrodes is 10 µm, in model 1.2 it is 5 µm and in model 1.3 the gap is 20 µm. See Figures 5.5, 5.6 and 5.7, respectively. (There is images only for DEP values providing high enough force for trapping.)

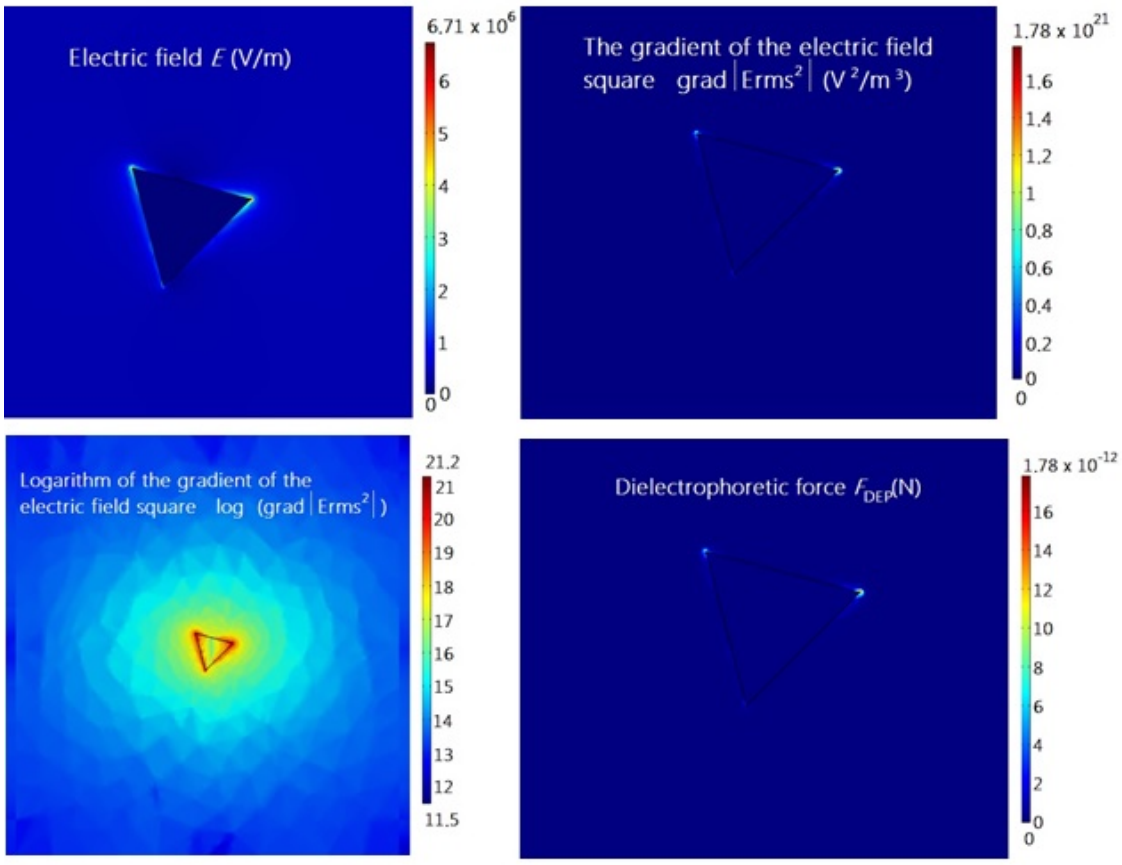

Figure 5.5: Electric field, the gradient of the field square, logarithm of the gradient of the field square and DEP force images for 12 V_{pp} for orientation 4 in model 1.1.

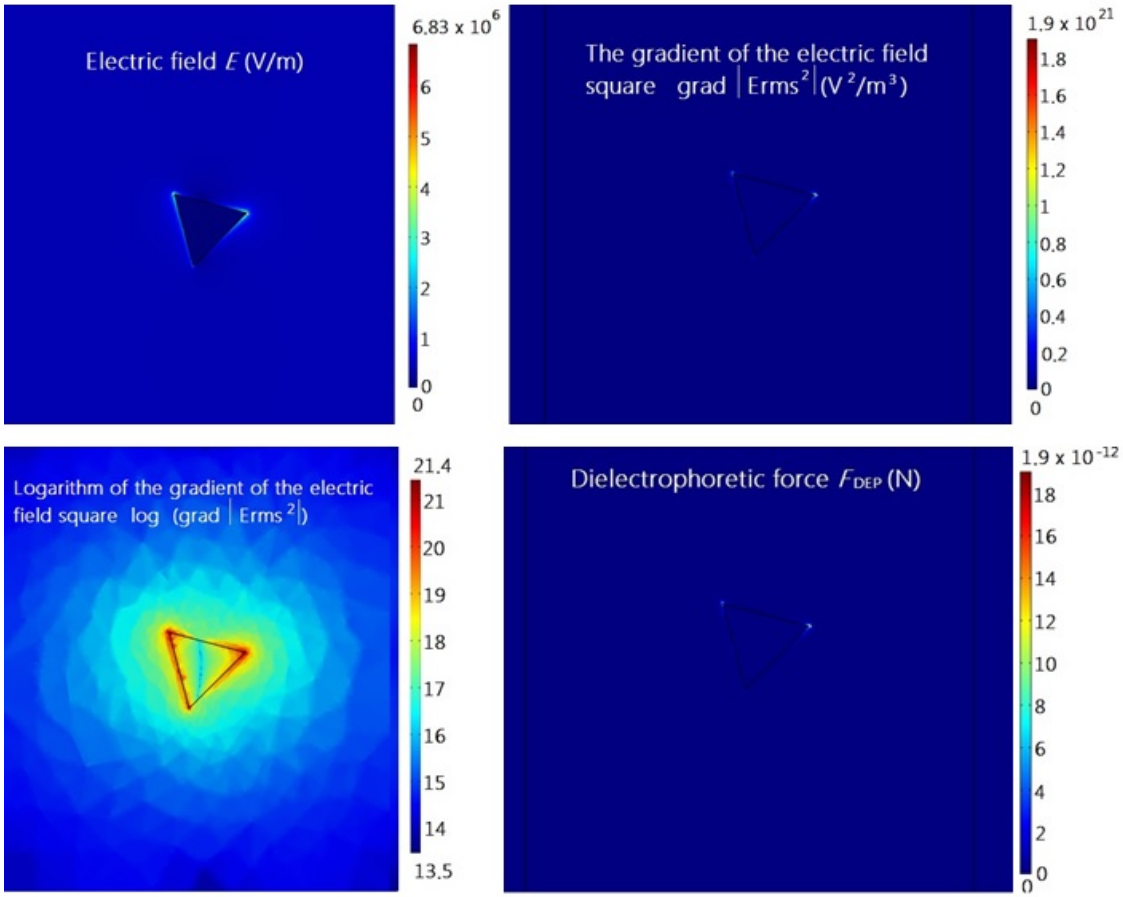

Figure 5.6: Electric field, the gradient of the field square, logarithm of the gradient of the field square and DEP force images for 7 V_{pp} for orientation 4 in model 1.2.

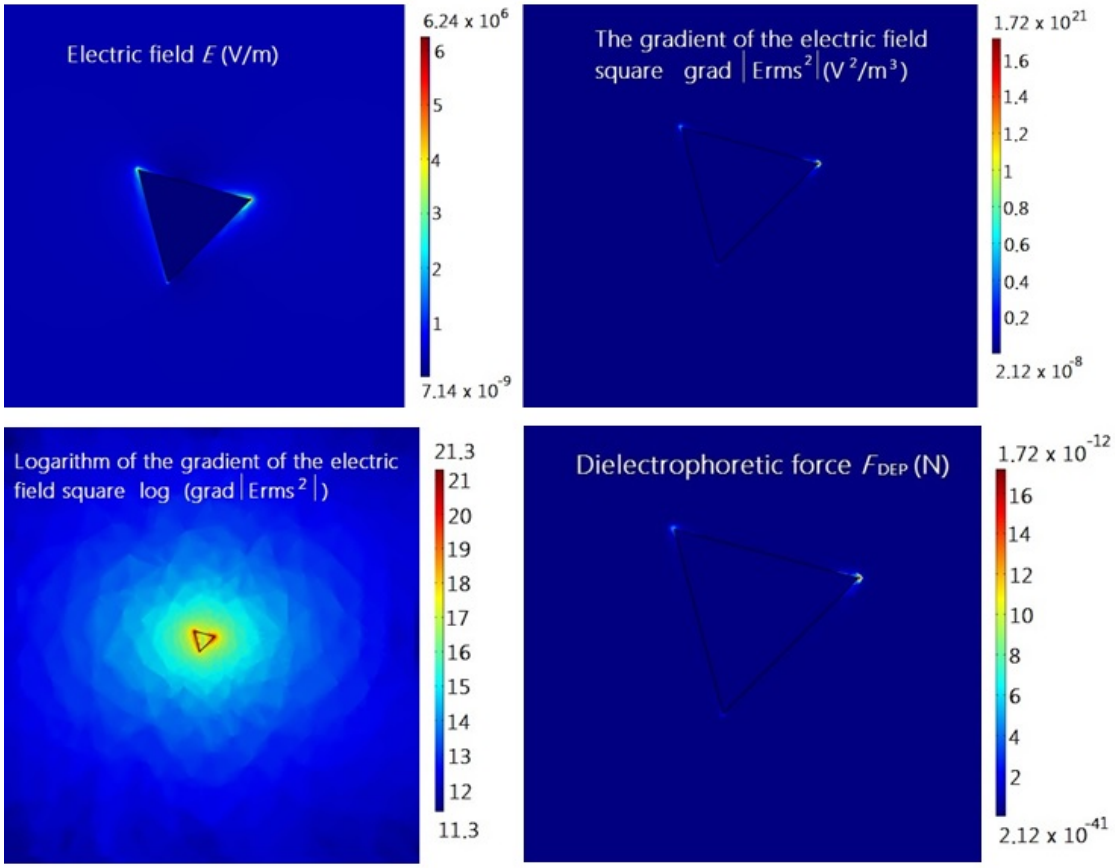

Figure 5.7: Electric field, the gradient of the field square, logarithm of the gradient of the field square and DEP force images for 21 V_{pp} for orientation 4 in model 1.3.

By comparing variations of model 1, it can be observed that the growing gap will raise the required voltage value, in order to obtain the required high DEP force. Simulation data can be seen in Appendixes C.2, C.3 and C.4.

5.2.2 Model 2

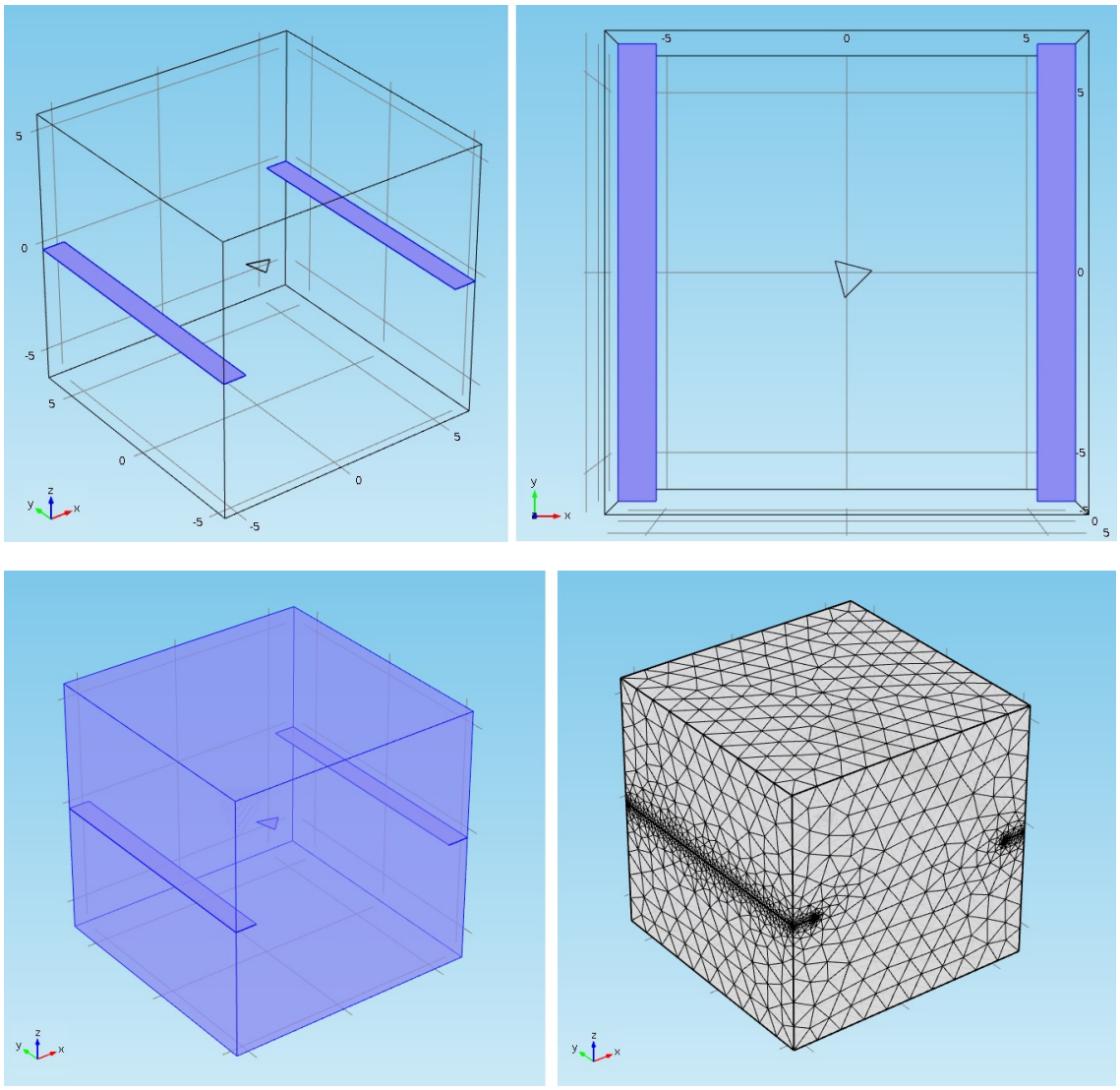

Figure 5.8: Model 2.1. has a cube with side length of 12 µm and electrodes are 1 µm wide. So, the gap between two electrodes is 10 µm.

In the model 2 the triangle is floating in water medium and electrodes with 1 µm width are now as thin as the triangle. In model 2.1 (Fig.5.8) the gap between the electrodes is 10 µm, in model 2.2 it is 5 µm and in model 2.3 the gap is 20 µm.

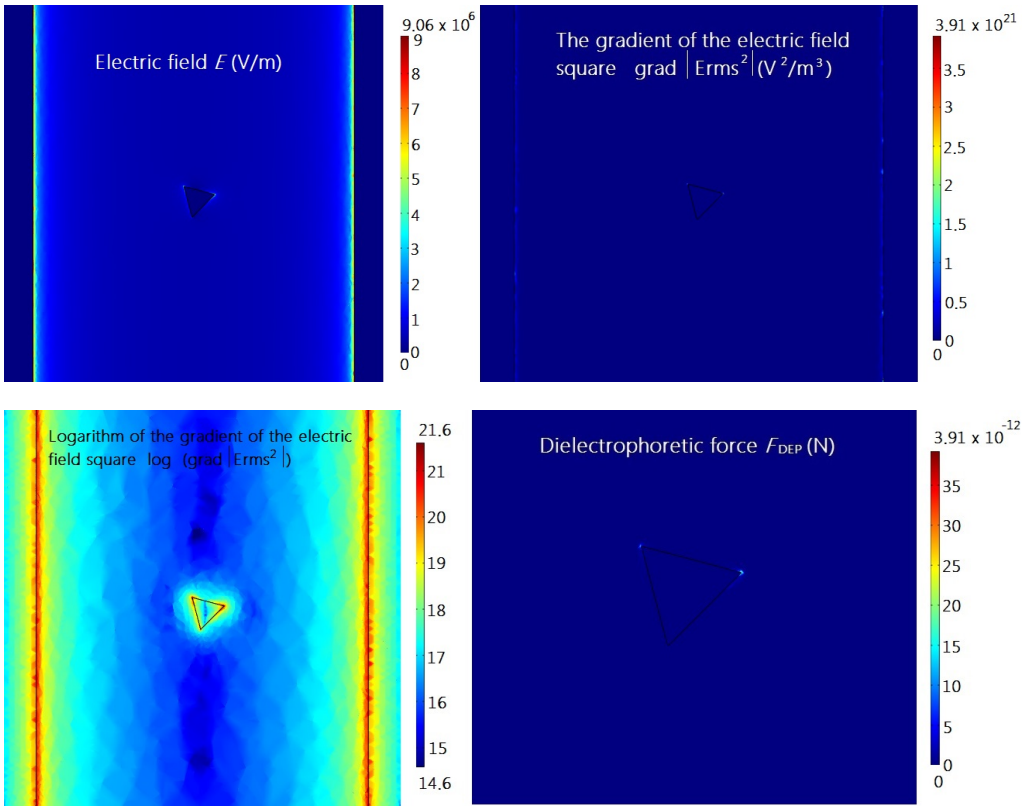

Figure 5.9: Electric field, the gradient of the field square, logarithm of the gradient of the field square and DEP force images for 20 V_{pp} for orientation 4 in model 2.1.

In model 2.1, the electrodes reached required DEP force already with 14 V_{pp} voltage, but the triangle reached required DEP force with 20 V_{pp} voltage (Fig.5.9). So, the electrodes start to collect oligos with lower voltage than the actual triangle.

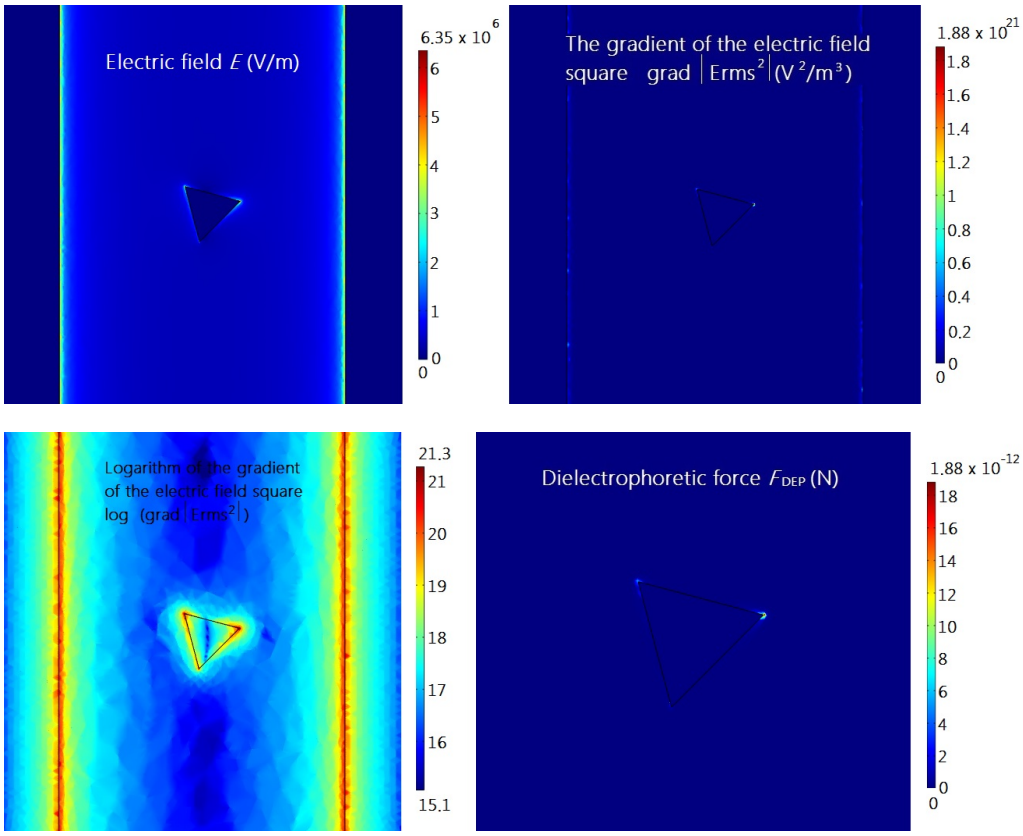

Figure 5.10: Electric field, the gradient of the field square, logarithm of the gradient of the field square and DEP force images for 8 V_{pp} for orientation 4 in model 2.2.

Now, in model 2.2 the triangle reached required DEP force already with 8 V_{pp} voltage, but the electrodes reached required DEP force with 15 V_{pp} voltage. So, the triangle start to collect oligos with lower voltage than the electrodes. This is good, because we want the oligos to be trapped only to triangles (Fig.5.10).

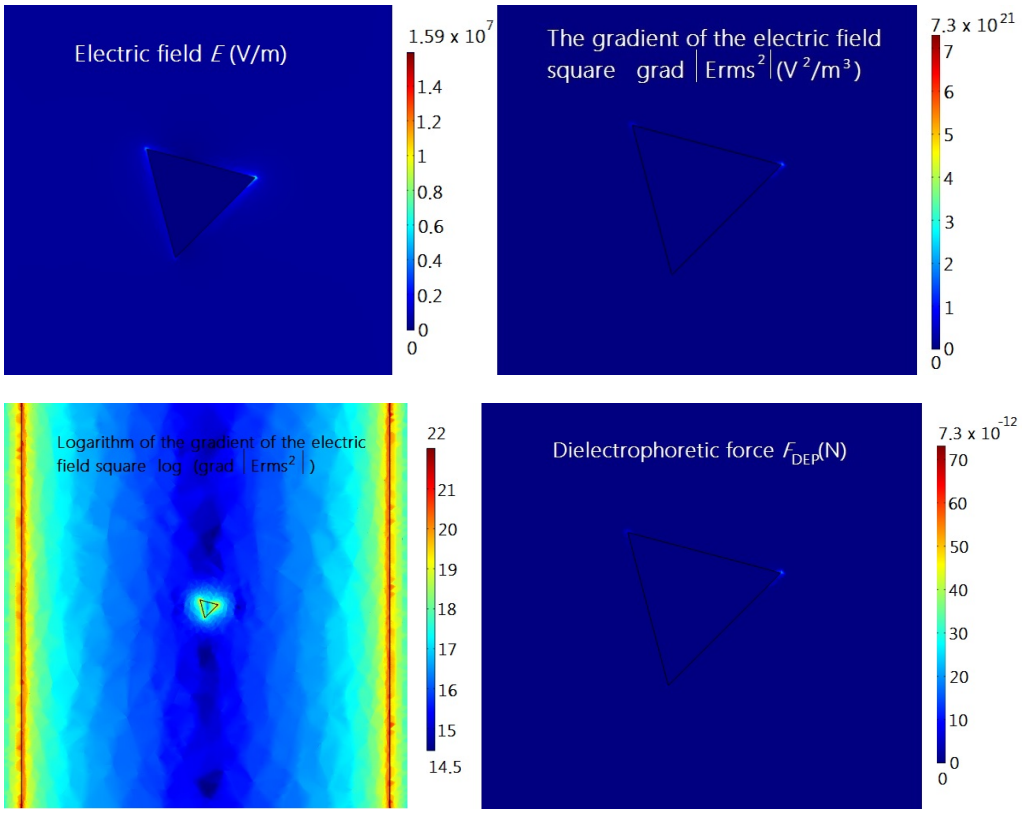

Figure 5.11: Electric field, the gradient of the field square, logarithm of the gradient of the field square and DEP force images for 42 V_{pp} for orientation 4 in model 2.3.

Again with wider gap of model 2.3, the required DEP force is achieved with different voltages in the electrodes and the triangle. The electrodes need 21 V_{pp} voltage and the triangle 42 V_{pp} (Fig.5.11). Simulation data of model 2 can be seen in Appendixes C.5, C.6 and C.7.

5.2.3 Model 3

The model 3 utilized finger-tip type of electrodes. In model 3.1 the gab between electrodes is 10 µm, in model 3.2 5 µm, in model 3.3 3 µm and in model 3.4 5 µm. The difference between models 3.2 and 3.4 is that the tip of the electrodes are sharper in model 3.4 than in model 3.2. For model 3 were looked only the best voltage value, which can be sufficient to achieve required DEP force. See Fig. 5.12.

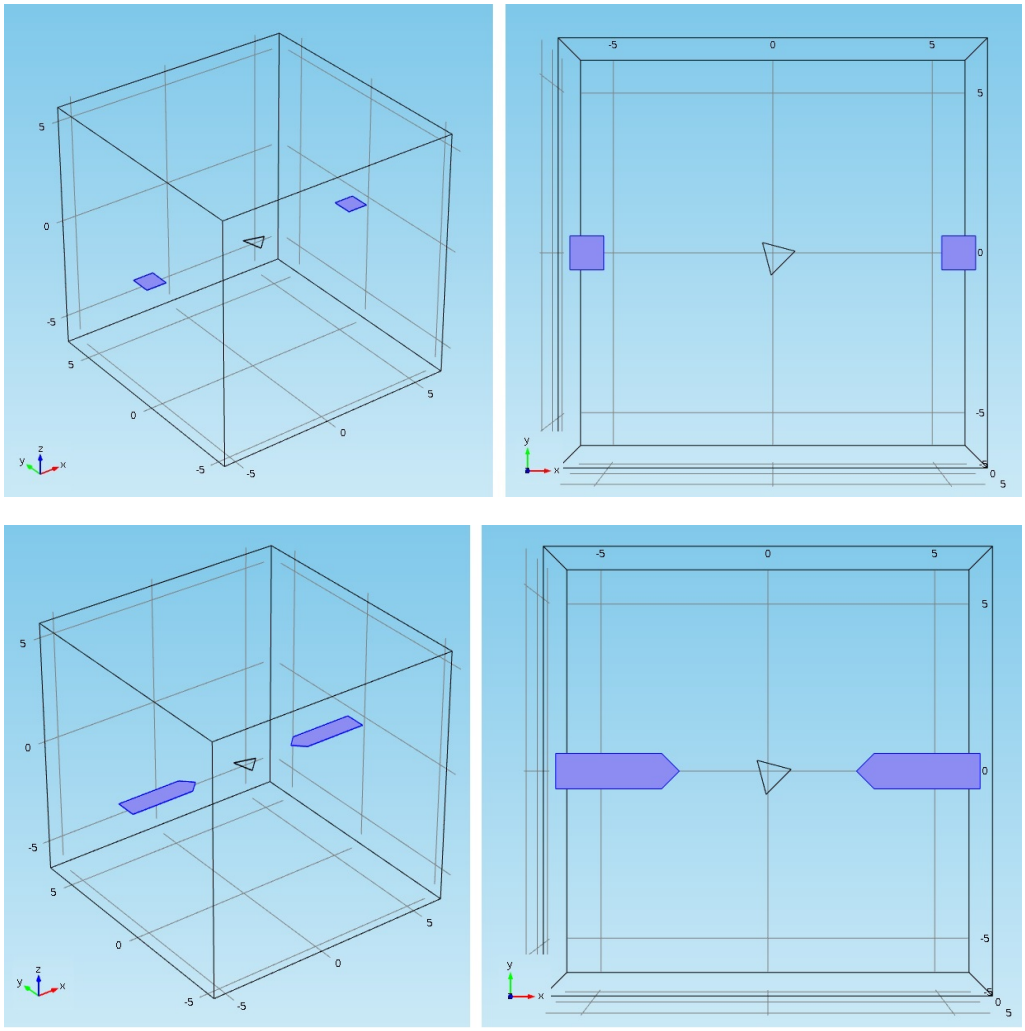

Figure 5.12: Model 3.1 and 3.4. Models have a cube with side length of 12 µm. For model 3.1 electrodes are 1 µm × 1 µm × 0.02 µm and for model 3.4 electrodes are 3.5 µm × 1 µm × 0.02 µm. So, the gap between two electrodes is 10 µm in model 3.1 and 5 µm in model 3.4.

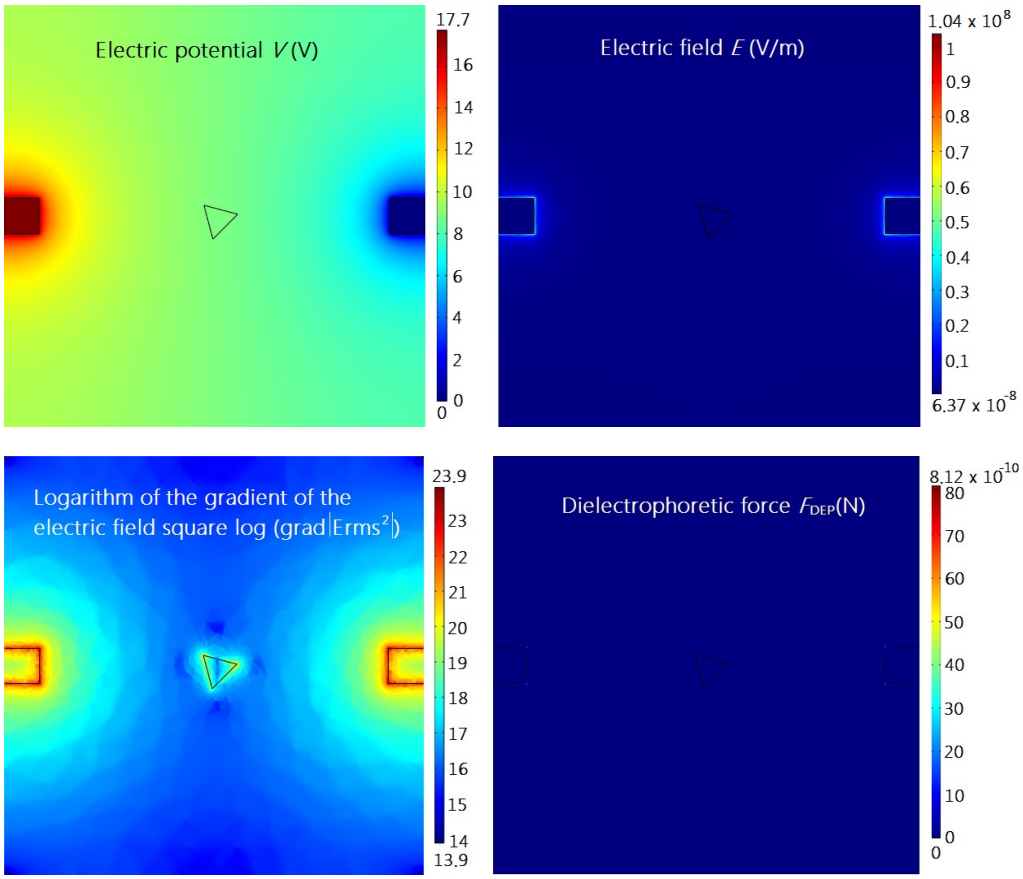

Figure 5.13: Electric potential, Electric field, logarithm of the gradient of the electric field square and DEP force images for 50 V_{pp} for orientation 4 in model 3.1.

The required DEP force is achieved with 3 V_{pp} voltage for electrodes and 50 V_{pp} voltage for triangle in model 3.1 (Fig.5.13).

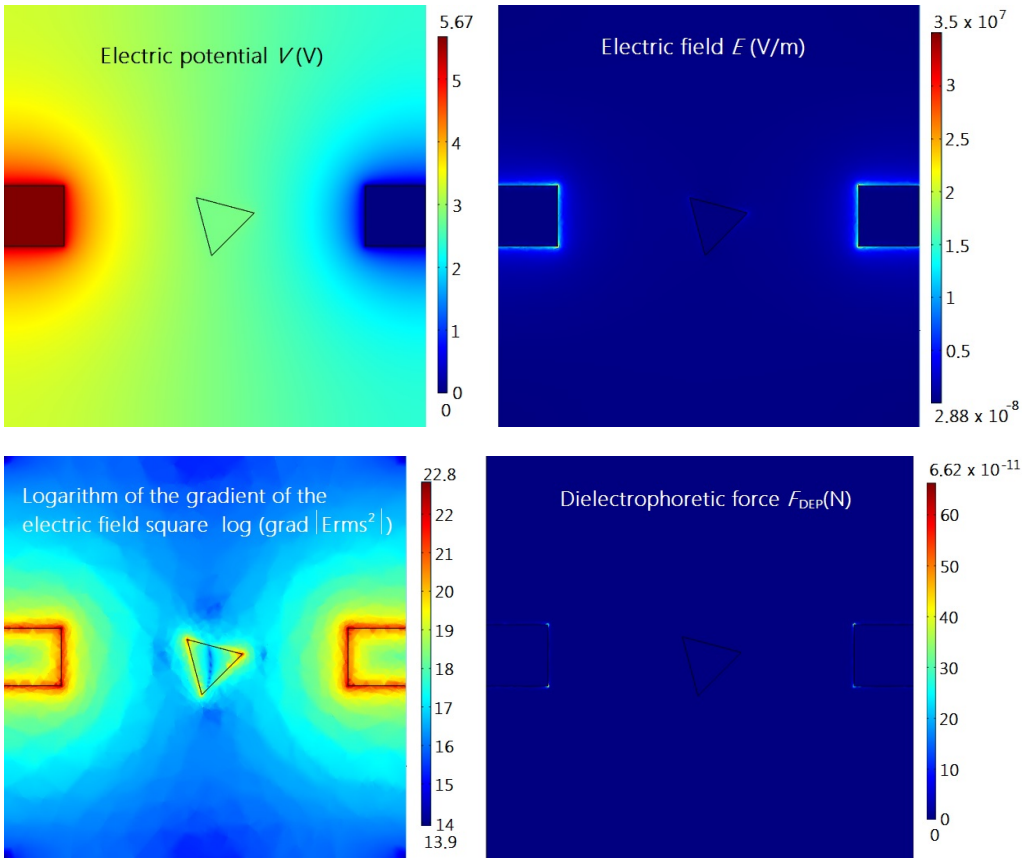

Figure 5.14: Electric potential, Electric field, logarithm of the gradient of the electric field square and DEP force images for 16 V_{pp} for orientation 4 in model 3.2.

The required DEP force is achieved with 3 V_{pp} voltage for electrodes and 16 V_{pp} voltage for triangle in model 3.2 (Fig.5.14).

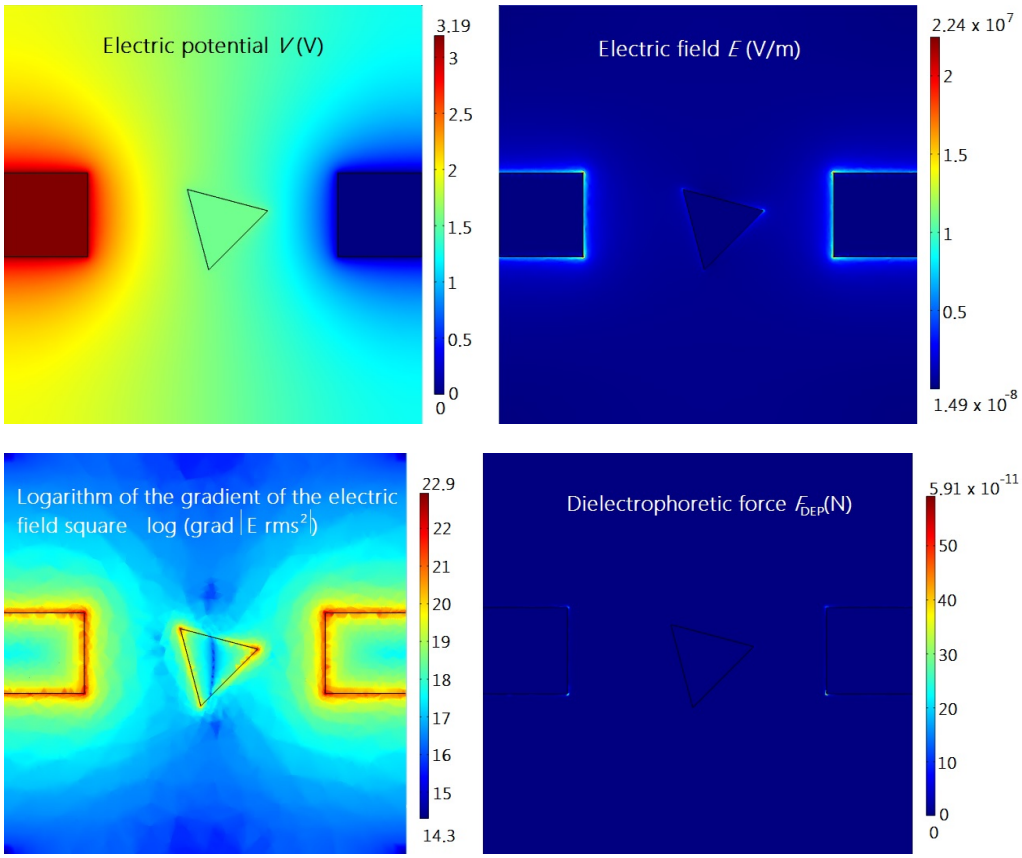

Figure 5.15: Electric potential, Electric field, logarithm of the gradient of the electric field square and DEP force images for 9 V_{pp} for orientation 4 in model 3.3.

The required DEP force is achieved with 2 V_{pp} voltage for electrodes and 9 V_{pp} for triangle in model 3.3 (Fig.5.15).

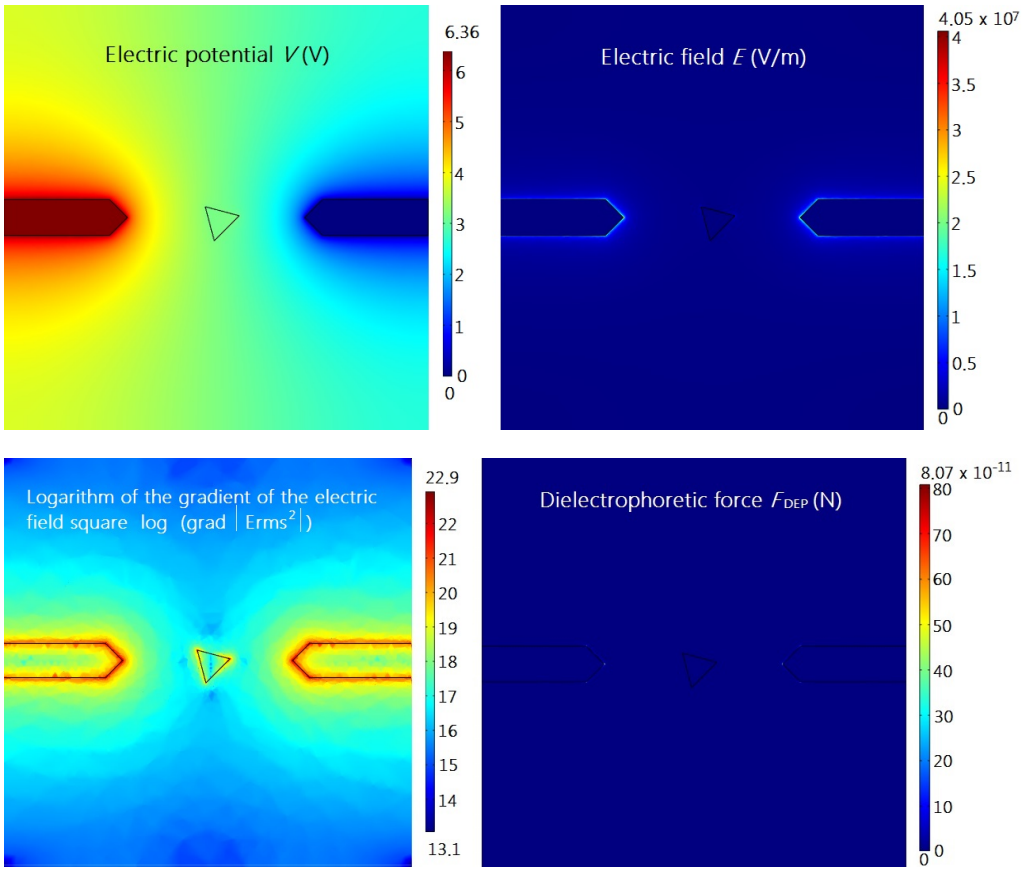

Figure 5.16: Electric potential, Electric field, logarithm of the gradient of the electric field square and DEP force images for 18 V_{pp} for orientation 4 in model 3.4.

The required DEP force is achieved with 3 V_{pp} voltage for electrodes and 18 V_{pp} voltage for triangle in model 3.4 (Fig.5.16).

Due to poor properties found on the simulations the model 3 was never tested experimentally.

5.2.4 Model 4

Design of the model 4 is shown on the figure 5.17 below and the results on the following figure 5.18. Now modeled is also the Silicon substrate and SiO_2 on top of it. Gap between electrodes is 10 µm.

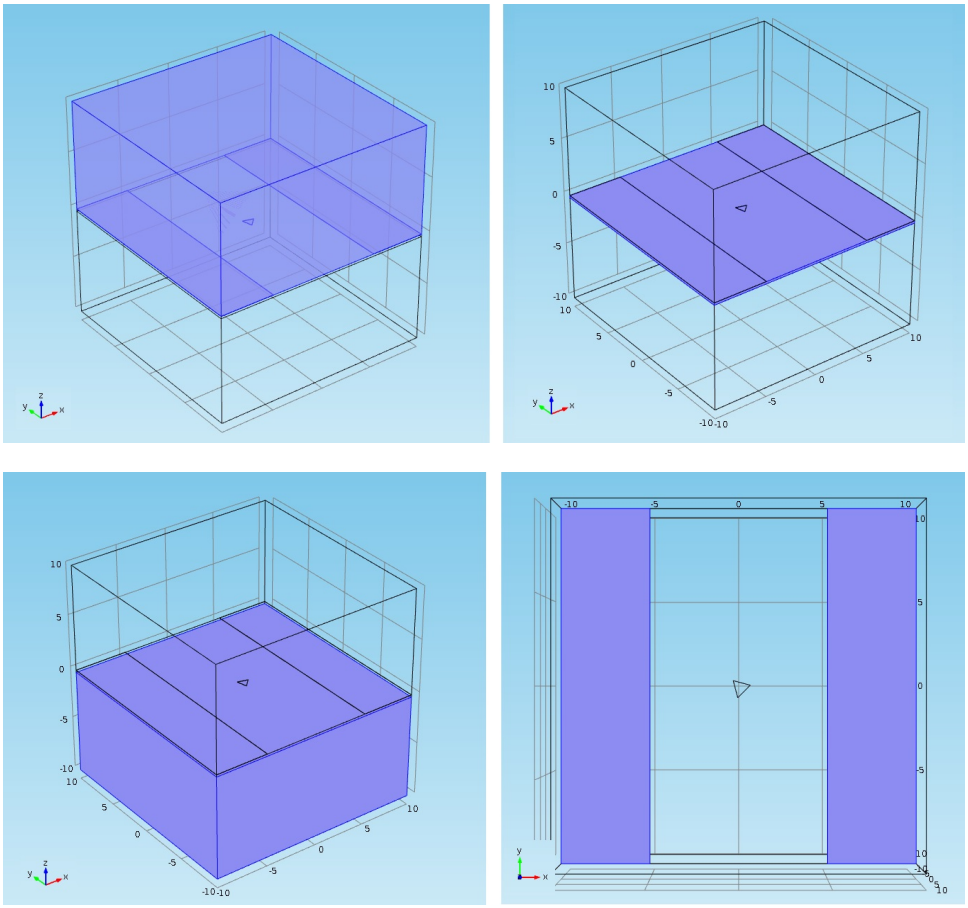

Figure 5.17: Model 4.1 has been built in a box with side length of 20 µm. Electrodes are now 5 µm × 20 µm × 0.02 µm large. Water medium is showed in the first image, 300 nm thick SiO_2-layer in the second image, Si-layer (it is now only 9.7 µm thick) in the third image and electrodes are showed in the last image.

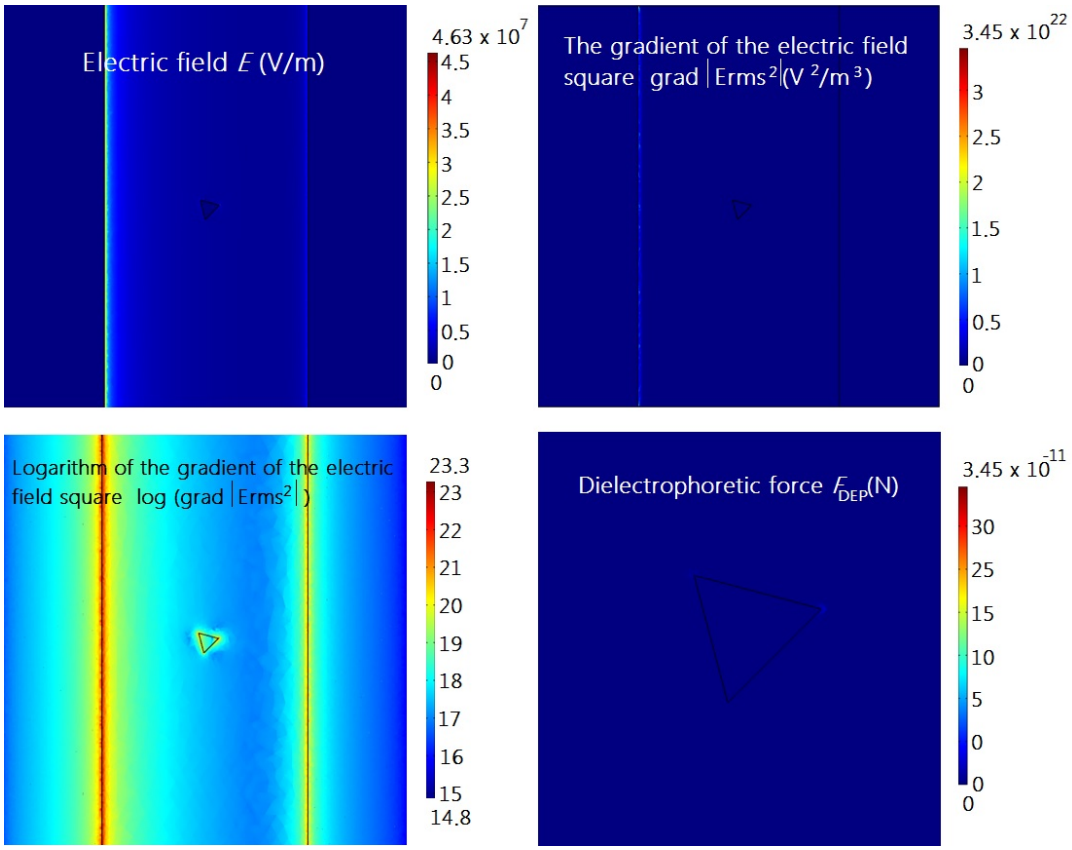

Figure 5.18: Electric field, the gradient of the electric field square, logarithm of the gradient of the electric field square and DEP force images for 60 V_{pp} for orientation 4 in model 4.1.

The required DEP force is achieved with 14 V_{pp} voltage for electrodes and 60 V_{pp} voltage for triangle in model 4.1 (Fig.5.18).

In model 4.1, the source electrode have much higher DEP force than the ground electrode, which is due to the silicon substrate below the SiO_2 layer.

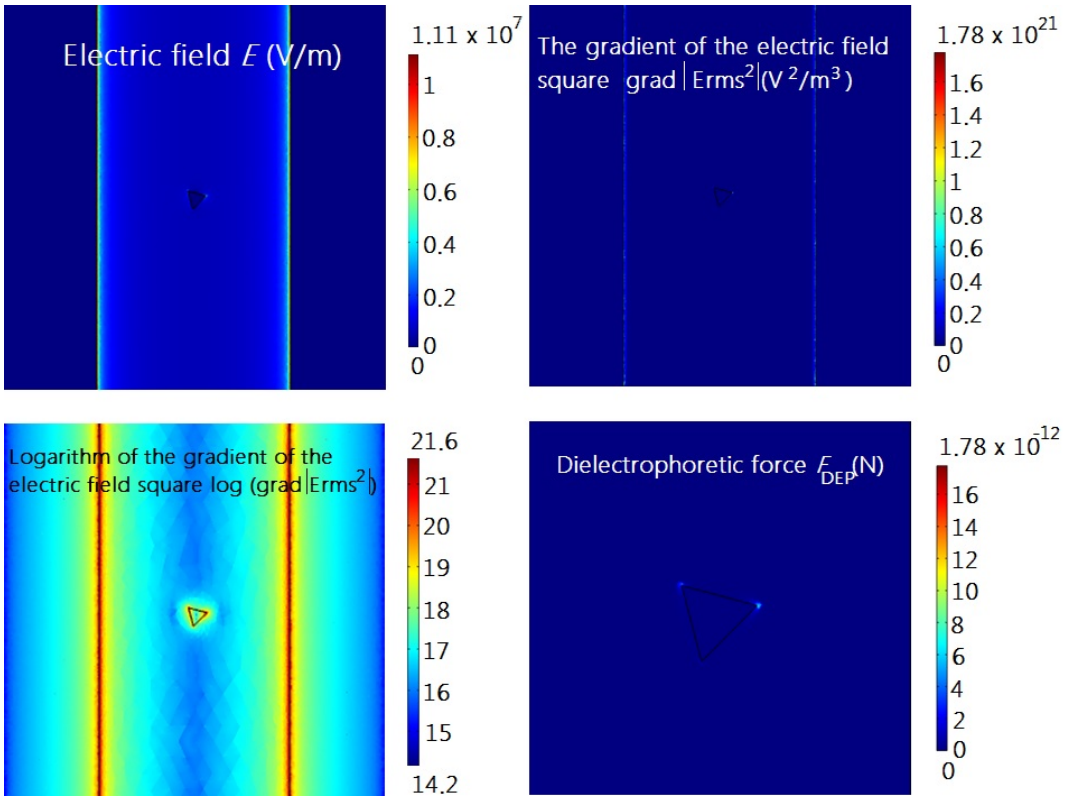

Figure 5.19: Electric field, the gradient of the electric field square, logarithm of the gradient of the electric field square and DEP force images for 30 V_{pp} for orientation 4 in model 4.2.

Model 4.2 has been built in the same way as model 4.1 (See Fig.5.17.), but now there is no SiO_2- and Si-layers. Instead, triangle and electrodes are on the 1 µm thick Si_3N_4-layer and under this layer is also water. The required DEP force is achieved with 30 V_{pp} voltage for electrodes and triangle in model 4.2 (Fig.5.19). By comparing model 4.1 to model 4.2, it can be seen, that in model 4.2 the DEP force of electrodes is symmetric and in model 4.1 it is asymmetric.

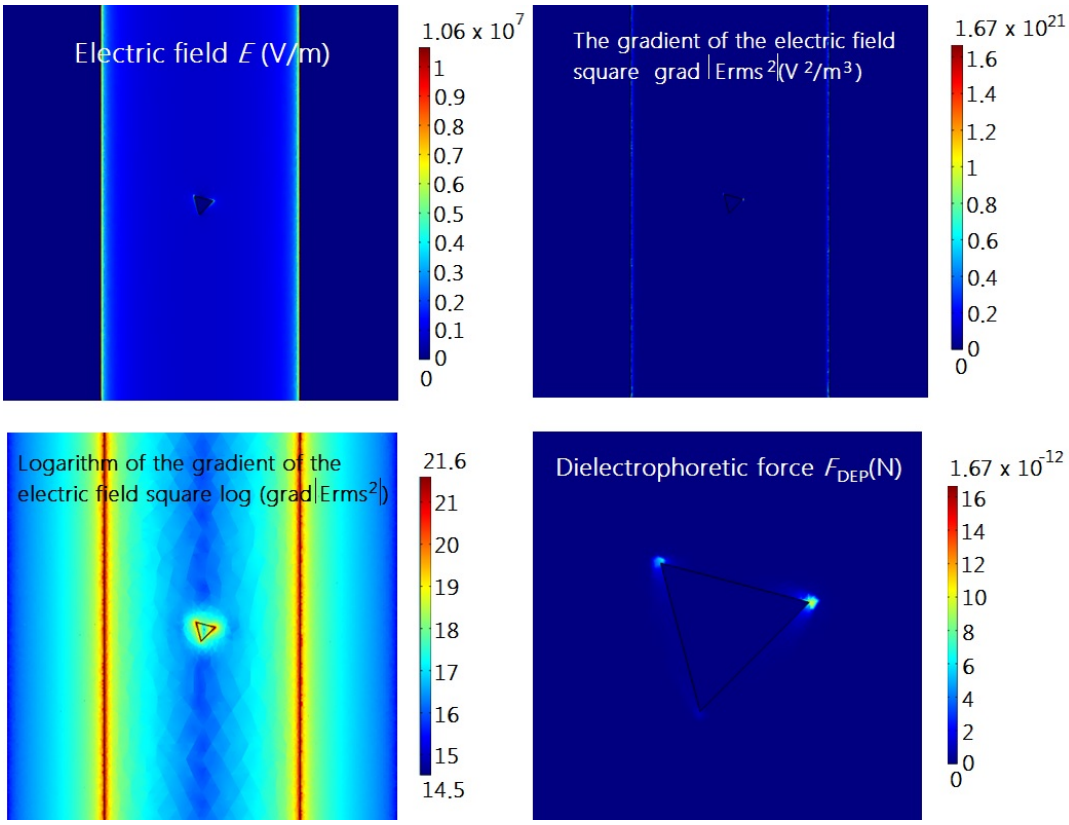

Figure 5.20: Electric field, the gradient of the electric field square, logarithm of the gradient of the electric field square and DEP force images for 34 V_{pp} for orientation 4 in model 4.3.

Model 4.3 has been built in the same way as model 4.2, but now in place of water there is air under Si_3N_4-layer. The required DEP force is achieved with 34 V_{pp} voltage for system in model 4.3 (Fig.5.20). Comparing models 4.2 and 4.3, it can be seen that with air-layer, we need higher voltage to achieve required DEP force. This is due to the fact that the permittivity value of water is much higher than air's.

Conclusions

Purpose of this study was to examine whether biomolecules can be trapped separately on the corners of triangular gold nanoparticles, or trapped at all by them. In this study single-stranded, thiol-modified and fluorescent-dye-labeled DNA strands were used. A variety of trapping systems and DEP parameters were used to find functional trapping system. The functionality of the systems were examined in both experimental and theoretical (simulations) way.

In the experimental review, the problem was the sudden disappearance, i.e. bleaching, of the fluorescence, which hindered the detection of the oligonucleotides. This is a known phenomenon and problem in all fluorescence imaging. Without the fluorescence, it was virtually impossible to detect these small molecules with these imaging methods, which have been used in this study.

In those samples, which were dried before imaging, only a little fluorescent was observed. Whereas, when the sample was still wet, more fluorescence was detected. During the live-DEP, it was also found that the magnitude of the voltage affected to the total concentration of the fluorescent. When the voltage increased over the 35 V_{pp}, then it was observed huge amount of the oligos. This is probably due to the fact that this high voltage generated "additional" flows to fluid, in which buoyancy is probably the reason for that the oligos were detected much more than before. The buoyancy raised oligos on the surface of the fluid (concentration of oligos is large on the surface part of the fluid), in which case also focus point of fluorescent changed little bit. This could explain, why is no longer seen oligos, when the electric field is switched off and the focus point is not changed.

Only during the live-DEP, it was experimentally observed, that the effect of the electric field get the oligos to gather to the triangles. When the voltage was 40 V_{pp}, these oligos formed "cloud" around the triangles and in some triangles it was also possible to see oligos in the corners of the triangles. Switching of the voltage induced the disappearance of the fluorescence again, which could be due to the fact that the oligos stay trapped in the triangles only when electric field is on. Therefore, turning off the electric field seems to release the oligos. This phenomenon is also talked in Ralph Hölzel's article (Trapping Single Molecules by Dielectrophoresis [25]), where he tells that switching off the field immediately releases the molecules

from electrodes and also fluorescence seems to disappear.

In the simulated systems it was compared, how different electrodes affect to the maximum DEP-force achieved on the corners of the triangles. The DEP-force was estimated to be large enough for trapping, when it was same as the Brownian force of the oligo. In this manner, it was estimated a minimum voltage at which the oligos should trap to the triangles. For aggregated oligos, the required voltage is lower, because the Brownian motion decrease, when the size of the molecule increase, while the DEP force simultaneously increase.

From the simulated models, the model 4.3 was observed (the most real situation) to give almost similar results as the experimental data. In this model, the required DEP-force was reached with 34 V_{pp} voltage and in the experimental situation with 40 V_{pp}.

It was experimentally observed, that the oligos are more gathering to the electrodes, which could be explained by the fact, that the required DEP-force is achieved already with lower voltages. This can be also seen in the simulations, where the DEP-force is higher in the electrodes than in the triangles with same value of voltage. Also, it seemed to affect, if there is window or silicon under the triangle. When the triangle was not on the window the oligos were observed to gather only in the electrodes. This can be explained by the silicon substrate acting as a additional grounding.

All in all, this study proves that the gold nano triangles can be used for trapping molecules. Three sensing tips provides greater opportunity to detect biomolecules, which offers the opportunity to build new biosensors. In the future, it could be possibly to use gold nano triangles as part of the nano-electronic circuits, where triangle could divid the input signal into two different directions. On the other hand, one possible application could be to use them for building molecular based materials, where the triangles could link fragments of the molecule networks together. This kind of biogoldnanofilm could be used to develop new types of optical applications.

Bibliography

[1] Victor E. Borisenko and Stefano Ossicini, *What is What in the Nanoworld*, Wiley-VHC (2012)

[2] Frank Schreiber, *Structure and growth of self-assembling monolayers*, Progress in Surface Science, 65, 151-256 (2000)

[3] Chad A. Mirkin and Robert L. Letsinger, *A DNA-based method for rationally assembling nanoparticles into macroscopic materials*, Nature, 382, 607-609 (1996)

[4] Paul W. K. Rothemund, *Folding DNA to create nanoscale shapes and patterns*, Nature, 440, 297-302 (2005)

[5] David L. Nelson and Michael M. Cox, *Lehninger Principles of Biochemistry*, W. H. Freeman (2004)

[6] Natalie Dias and C. A. Stein, *Antisense Oligonucleotides: Basic Concepts and Mechanisms*, Mol. Cancer. Ther. 1, 347-355 (2002)

[7] Jose V. Bonilla and G. Susan Srivatsa, *Handbook of Analysis of Oligonucleotides and Related Products*, CRC Press Taylor & Francis Group (2011)

[8] atdbio -website, http://www.atdbio.com/ (2014)

[9] R. G. Enders, D. L. Cox and R. R. P. Singh, *The request for high conductance DNA*, Rev. Mod. Phys., 76, 197-214 (2004)

[10] D. Porath, G. Cuniberti and R. Di Felice, *Charge transport in DNA-based devices*, Top. Curr. Chem., 237, 183-228 (2004)

[11] Xuefeng Guo, Alon A. Gorodetsky, James Hone, Jacqueline K. Barton and Colin Nuckolls, *Conductivity of a single DNA duplex bridging a carbon nanotube gap*, Nature, 3, 163-167 (2008)

[12] Irena Kratochvílová, Tatiana Todorciuc, et.al., *Charge Transport in DNA Oligonucleotides with Various Base-Pairing Patterns*, J. Phys. Chem. B 114, 5196-5205 (2010)

[13] Cees Dekker and Mark A. Ratner, *Electronic properties of DNA*, Physics World, 14, 29-33 (2001)

[14] Danny Porath, Alexey Bezryadin, Simon de Vries and Cees Dekker, *Direct measurement of electrical transport through DNA molecules*, Nature, 403, 635-638 (2000)

[15] Hans-Achim Wagenknecht, *Charge Transfer in DNA: From Mechanism to Application*, WILEY-VCH (2005)

[16] Chien-Ying Tsai, Tien-Li Chang, Long-Sheng Kuo and Ping-Hei Chen, *Detection of electrical characteristic of DNA strands immobilized on self-assembled multilayer gold nanoparticles*, Appl. Phys. Lett. 89, 203902 (2006)

[17] Anton Kuzyk, *Dielectrophoresis at the nanoscale*, Electrophoresis, 32, 2307-2313 (2011)

[18] Jaime Castillo-León, Winnie Edith Svendsen and Maria Dimaki, *Micro and Nano Techniques for the Handling of Biological Samples*, CRC Press (2012)

[19] Marc J. Madou, *Fundamentals of Microfabrication: The Science of Miniaturization*, CRC Press (2002)

[20] David J. Bakewell, Nuria Vergara-Irigaray and David Holmes, *Dielectrophoresis of Biomolecules*, Nanotechnol Nanomed 1 (1), 1003 (2013)

[21] Cornelius F. Ivory and Soumya K. Srivastava, *Direct current dielectrophoretic simulation of proteins using an array of circular insulating posts*, Electrophoresis, 32, 2323-2330 (2011)

[22] Lifeng Zheng, James P. Brody and Peter J. Burke, *Electronic manipulation of DNA, proteins, and nanoparticles for potential circuit assembly*, Biosensors and Bioelectronics, 20, 606-619 (2004)

[23] Veikko Linko, Jenni Leppiniemi, Boxuan Shen, Einari Niskanen, Vesa P. Hytönen and J. Jussi Toppari, *Growth of immobilized DNA by polymerase: bridging nanoelectrodes with individual dsDNA molecules*, Nanoscale, 3, 3788-3792

[24] Sampo Tuukkanen, Anton Kuzyk, J Jussi Toppari, Hannu Häkkinen, Vesa P Hytönen, Einari Niskanen, Marcus Rinkiö and Päivi Törmä, *Trapping of 27 bp-8 kbp DNA and immobilization of thiol-modified DNA using dielectrophoresis*, Nanotechnology, 18, 295204 (2007)

[25] Ralph Hölzel, Nils Calander, Zackary Chiragwandi, Magnus Willander and Frank F. Bier, *Trapping Single Molecules by Dielectrophoresis*, Am. Phys. Soc. PRL, 95, 128102 (2005)

[26] Benjamin G. Hawkins and Brian J. Kirby, *Electrothermal flow effects in insulating (electrodeless) dielectrophoresis systems*, Electrophoresis, 31, 3622-3633 (2010)

[27] Sriram Sridharan, Junjie Zhu, Guoqing Hu and Xiangchun Xuan, *Joule heating effects on electroosmotic flow in insulator-based dielectrophoresis*, Electrophoresis, 32, 2274-2281 (2011)

[28] A. González, A. Ramos, H. Morgan, N. G. Green and A. Castellanos, *Electrothermal flows generated by alternating and rotating electric fields in microsystems*, J. Fluid. Mech., 564, 415-433 (2006)

[29] Ciprian Iliescu, Guillaume Tresset and Guolin Xu, *Dielectrophoretic field-flow method for separating particle populations in a chip with asymmetric electrodes*, Biomicrofluidics, 3, 044104 (2009)

[30] Lenntech, Water Treatment Solutions -website, http://www.lenntech.com/applications/ultrapure/conductivity/water-conductivity.htm (2014)

[31] Rafael Tadmor, Ernesto Hernández-Zapata, Nianhuan Chen, Philip Pincus and Jacob N. Israelachvili, *Debye Length and Double-Layer Forces in Polyelectrolyte Solutions*, Macromolecules, 35, 2380-2388 (2002)

[32] N. G. Green, A. Ramos, A. Conzález, H. Morgan and A. Castellanos, *Fluid flow induced by nonuniform ac electric fields in electrolytes on microelectrodes. III. Observation of streamlines and numerical simulation*, Phys. Rev. E, 66, 026305 (2002)

[33] Doh-Hyoung Lee, Chengjie Yu, Elisabeth Papazoglou, Bakhtier Farouk and Hongseok M. Noh, *Dielectrophoretic particle-particle interaction under AC electrohydrodynamic flow conditions*, Electrophoresis, 32, 2298-2306 (2011)

[34] Adrian Bejan and Allan D. Kraus, *Heat Transfer Handbook*, WILEY (2003)

[35] V. Maudgal and Y. Joshi, *Numerical Simulation of Natural Convection Cooled Electronic Enclosures*, Electronic Components and Technology Conference, 45th, 1166-1173 (1995)

[36] Tanja Andrejeff, *Gold triangles by lithography*, Research Training, University of Jyväskylä, Department of Physics (2014)

Part III

Appendixes

Appendix A

Oligonucleotides

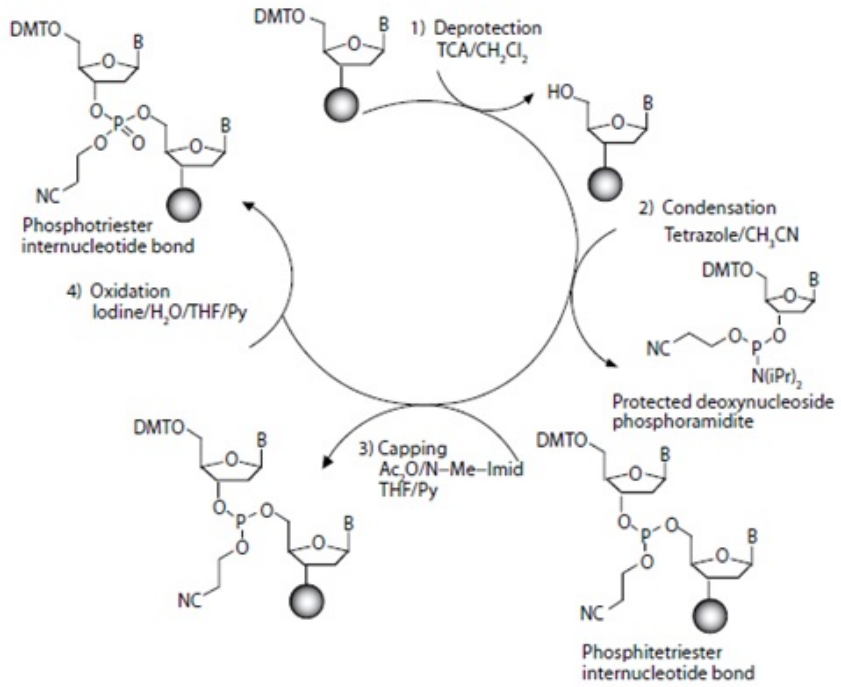

Figure A.1: The synthesis cycle of preparing oligonucleotides using phosphoramidite chemistry on controlled pore glass supports [7].

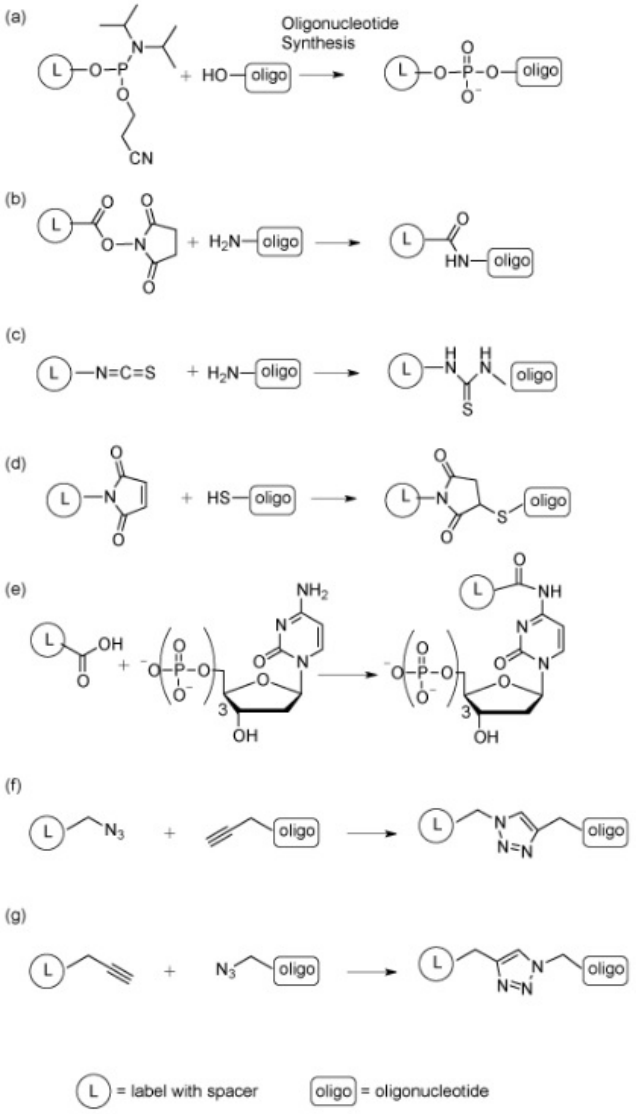

Figure A.2: Methods of oliogonucleotide labelling. (a) Reaction of a phosphoramidite derivative of the labelling group with the oligo during solid phase synthesis. (b-c) Reaction of a free amino group on an oligo with an N-hydroxysuccinimide ester or other activated carboxyl group. (d) Reaction of thiol-modified oligo with an α, β-unsaturated ketone. (e) Reaction of an amino-modified nucleoside triphosphate with a caboxy-activated label, and subsequent incorporation of the labelled triphosphate into DNA. (f) Reaction of an alkyne-modified oligo with an azide-modified label. (g) Reaction of an azide-modified oligo with an alkyne-modified label [8].

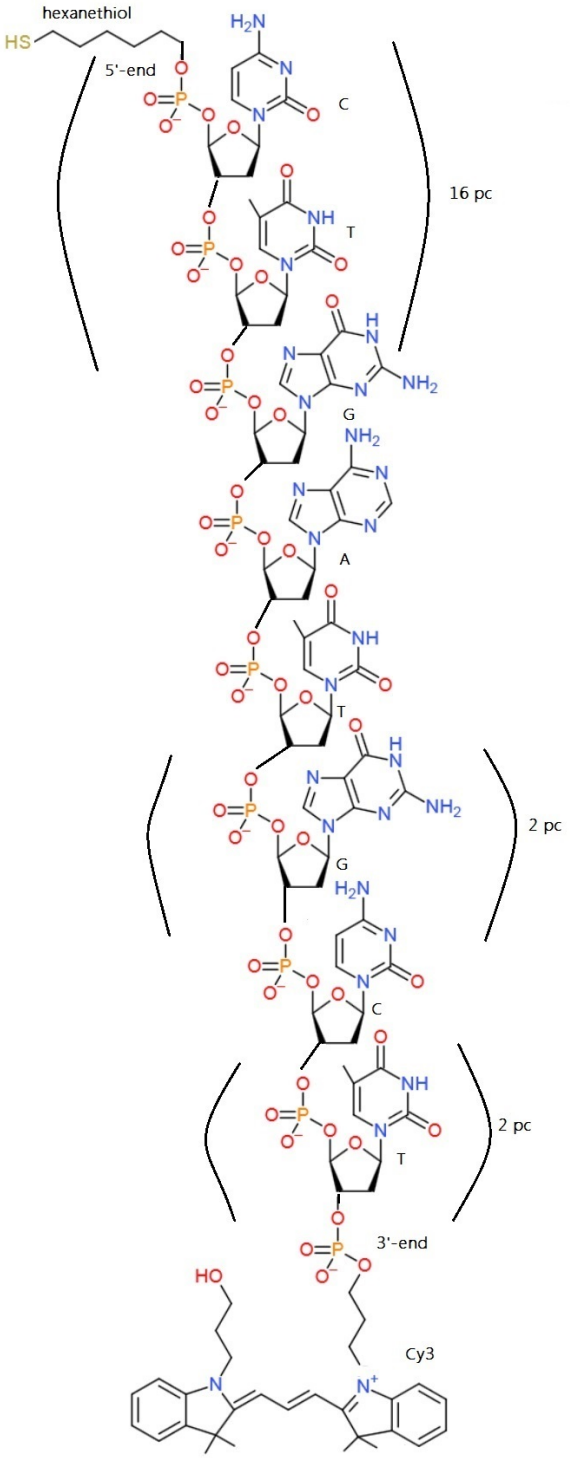

Figure A.3: Structure of thiol-modified and Cy3-dye labeled oligo.

Appendix B

Experimental data and images

Table B.1: Dilutions and trapping set ups for triangles with arrows system. (Randomly = oligos are all over the place.)

Sample	Cy3/Cy5	Dilution	DTT	f (MHz)	V_{pp} (V)	t (min)	Annotation
1	Cy5	1:100	-	1	20	30	Triangles inside bubbles
2	Cy3	1:100	-	1	20	45	Randomly
3	Cy3	1:3000	-	1	20	45	Not trap
4	Cy3	1:100	1:25	1	20	30	Not trap
5	Cy3	1:100	1:100	1	20	45	Not trap
6	Cy3	1:100	1:40	1	20	45	Randomly
7	Cy3	1:1000	1:1000	10	20	45	Near to couple of triangles
8	Cy3	1:1000	1:250	10	20	45	Too much oligos
9	Cy3	1:1000	1:250	0.1	20	45	Too little oligos

Table B.2: Dilutions and trapping set ups for triangles with electrodes system. Now all oligo-dilutions included only Cy3-fluorecent dye.

Sample	Dilution	DTT	f (MHz)	V_{pp} (V)	t (min)	Annotation
1	1:1000	1:200	1	5	15	Only on the electrodes
2	1:1000	1:200	1	5	10	Randomly
3	1:100000	1:20000	1	5	20	Randomly
4	1:10000	1:2000	10	3	5	Randomly
5	1:10000	1:2000	1	5	10	Too many oligos
6	1:100000	1:20000	1	5	10	Too little oligos

Table B.3: Dilutions and trapping set ups for triangles with electrodes and window system. All oligo-dilutions included only Cy3-fluorecent dye. In sample 13 and 15 oligos were diluted to buffer: Buffer 1 : 3 mM Hepes/ 4 mM NaOH and Buffer 2: 6.5 mM Hepes/NaOH.

Sample	Dilution	DTT	f (MHz)	V_{pp} (V)	t (min)	Annotation
1	1:50	-	1	20	10	Very little oligos
2	1:50	-	1	40	15	Oligos were aggregated
3	1:50	1:50	1	40	15	With DTT less aggregated
4	1:50	1:10	10	40	15	One triangle was surrounded by oligos
5	1:100	1:20	20	40	15	Very little oligos
6	1:50	1:10	20	40	15	Oligos were sticked to trash
7	1:50	1:10	15	40	15	Gap 20 µm
8	1:50	1:10	15	40	15	The second electrode were damaged
9	1:50	1:10	12.5	40	15	Both electrodes were damaged
10	1:50	1:10	10	30	15	Not trap to the triangle
11	1:50	1:10	10	34	25	Not trap to the triangle
12	1:25	1:5	10	40	15	Gap 20 µm
13	1:25	1:13	10	40	15	Diluted to buffer 1
14	1:50	1:25	10	40	15	No cleaning, sample still wet
15	1:50	1:25	10	40	15	Diluted to buffer 2
16	1:50	1:25	10	13	20	Few oligos near one or two triangle

Table B.4: Dilutions and trapping set ups for live-DEP. Trapping and video filming took about half an hour for each sample.

Sample	Dilution	DTT	f (MHz)	V_{pp} (V)	Annotation
1	1:50	1:25	10	10 - 20	Oligos were aggregated
2	1:50	1:25	10	10 - 20	One electrode unstacked during trapping
3	1:50	1:25	10	20 - 40	Didn't see any oligos → something wrong
4	1:50	1:25	10	30 - 50	The sample was dried up quickly
5	1:50	1:25	10	20 - 40	Around the triangles were formed oligo "clouds"

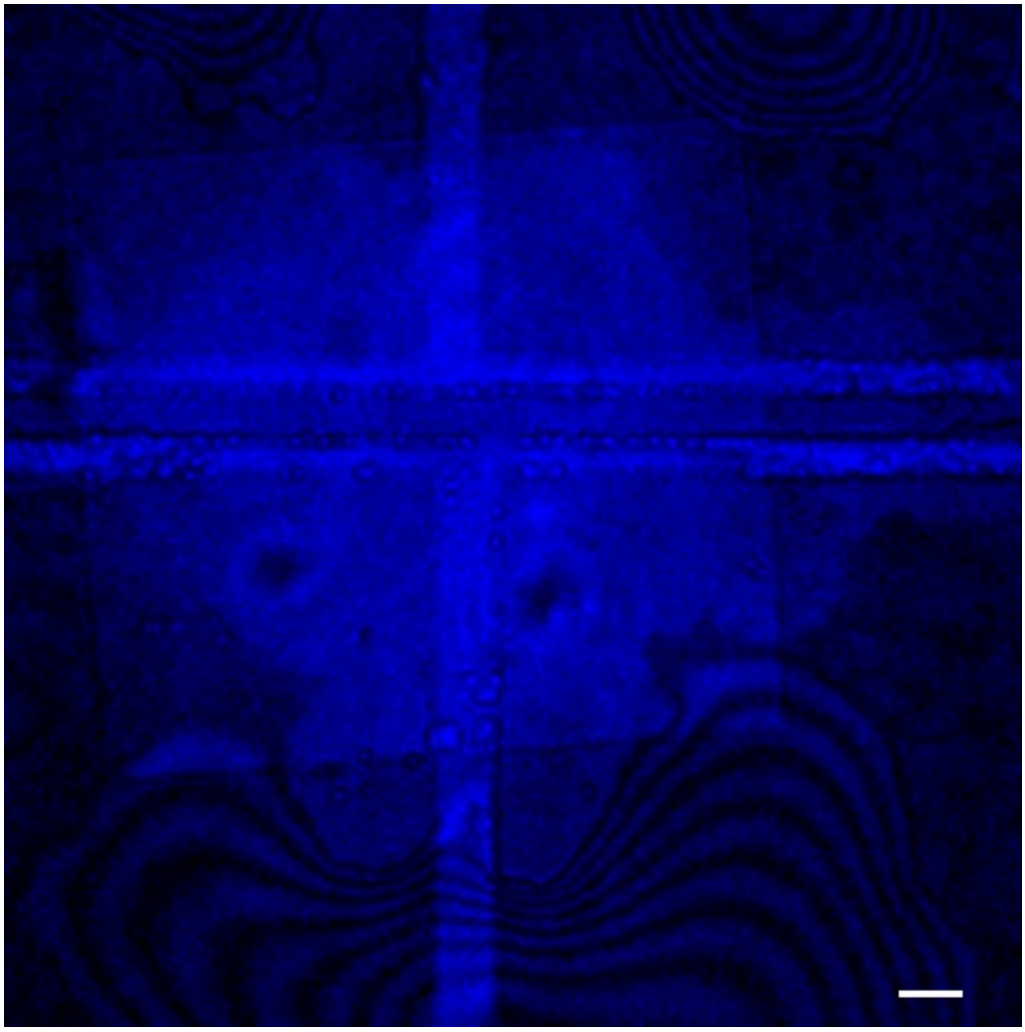

Figure B.1: Confocal microscope image of triangles with electrodes and window system. After live-DEP, the sample looks like this. We can see some drying trails. White scale par in image is about 10 µm.

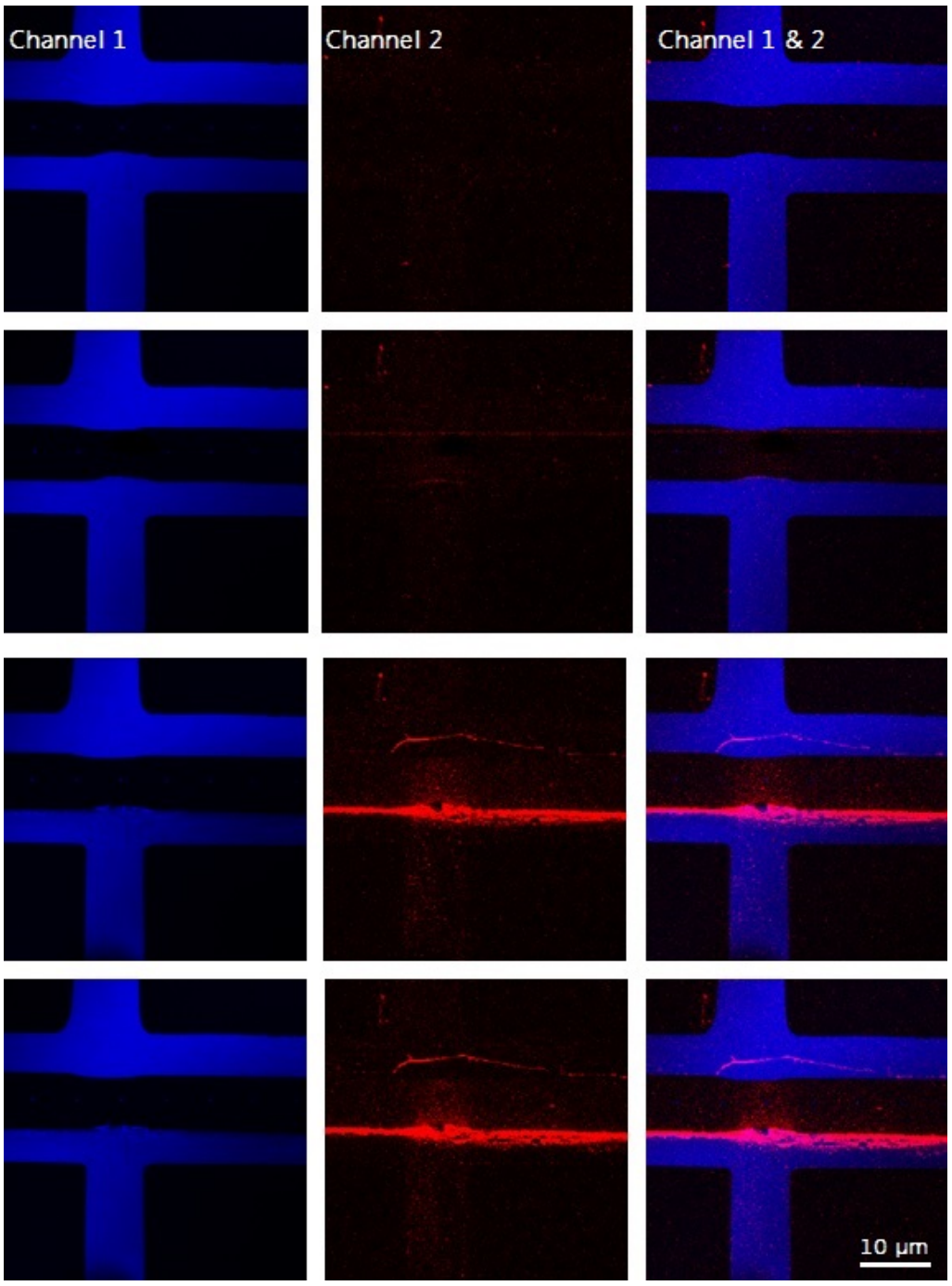

Figure B.2: Confocal microscope image of system, when electrode breaks.

Appendix C

Simulations data and images

Table C.1: COMSOL data for model 1.1. Electric field, the maximum of gradient of the square of the electric field, logarithm of previous and maximum DEP force values for different orientation with different voltages.

Orientation	V_{pp} (V)	V_{rms} (V)	E (V/m)	$\nabla\|E^2\|$ (V^2/m^3)	log $\nabla\|E^2\|$	F_{dep} (N)
1	1	0.35	4.67×10^5	9.96×10^{18}	19.1	9.96×10^{-15}
2	1	0.35	5.07×10^5	8.09×10^{18}	19.1	8.09×10^{-15}
3	1	0.35	5.87×10^5	1.14×10^{19}	19.1	1.14×10^{-14}
4	1	0.35	5.59×10^5	1.24×10^{19}	19.1	1.24×10^{-14}
1	5	1.77	2.38×10^6	2.49×10^{20}	20.5	2.49×10^{-13}
2	5	1.77	2.54×10^6	2.02×10^{20}	20.5	2.02×10^{-13}
3	5	1.77	2.94×10^6	2.84×10^{20}	20.5	2.84×10^{-13}
4	5	1.77	2.80×10^6	3.09×10^{20}	20.5	3.09×10^{-13}
1	10	3.54	4.76×10^6	9.96×10^{20}	21.1	9.96×10^{-13}
2	10	3.54	5.07×10^6	8.09×10^{20}	21.1	8.09×10^{-13}
3	10	3.54	5.87×10^6	1.14×10^{21}	21.1	1.14×10^{-12}
4	10	3.54	5.59×10^6	1.24×10^{21}	21.1	1.24×10^{-12}
1	15	5.31	7.14×10^6	2.24×10^{21}	21.4	2.24×10^{-12}
2	15	5.31	7.61×10^6	1.82×10^{21}	21.4	1.82×10^{-12}
3	15	5.31	8.81×10^6	2.56×10^{21}	21.5	2.56×10^{-12}
4	15	5.31	8.39×10^6	2.78×10^{21}	21.4	2.78×10^{-12}
1	20	7.08	9.52×10^6	3.98×10^{21}	21.7	3.98×10^{-12}
2	20	7.08	1.01×10^7	3.23×10^{21}	21.7	3.23×10^{-12}
3	20	7.08	1.17×10^7	4.55×10^{21}	21.7	4.55×10^{-12}
4	20	7.08	1.12×10^7	4.94×10^{21}	21.7	4.94×10^{-12}
1	40	14.2	1.90×10^7	1.59×10^{22}	22.3	1.59×10^{-11}
2	40	14.2	2.03×10^7	1.29×10^{22}	22.3	1.29×10^{-11}
3	40	14.2	2.35×10^7	1.82×10^{22}	22.3	1.82×10^{-11}
4	40	14.2	2.24×10^7	1.98×10^{22}	22.3	1.98×10^{-11}

Table C.2: COMSOL Multiphysics simulation data for model 1.1. Electric field, the maximum of the gradient of the electric field square, logarithm of the gradient of the electric field square and the maximum DEP force values for orientation 4 with different voltages.

V_{pp} (V)	V_{rms} (V)	E (V/m)	$\nabla\|E^2\|$ (V^2/m^3)	log $\nabla\|E^2\|$	F_{dep} (N)
1	0.35	5.59×10^5	1.24×10^{19}	19.1	1.24×10^{-14}
5	1.77	2.80×10^6	3.09×10^{20}	20.5	3.09×10^{-13}
10	3.54	5.59×10^6	1.24×10^{21}	21.1	1.24×10^{-12}
15	5.31	8.39×10^6	2.78×10^{21}	21.4	2.78×10^{-12}
20	7.08	1.12×10^7	4.94×10^{21}	21.7	4.94×10^{-12}
40	14.2	2.24×10^7	1.98×10^{22}	22.3	1.98×10^{-11}

Table C.3: COMSOL Multiphysics simulation data for model 1.2.

V_{pp} (V)	V_{rms} (V)	E (V/m)	$\nabla\|E^2\|$ (V^2/m^3)	log $\nabla\|E^2\|$	F_{dep} (N)
1	0.35	9.76×10^5	3.88×10^{19}	19.7	3.88×10^{-14}
5	1.77	4.88×10^6	9.70×10^{20}	21.1	9.70×10^{-13}
10	3.54	9.76×10^6	3.88×10^{21}	21.7	3.88×10^{-12}
15	5.31	1.46×10^7	8.73×10^{21}	22.1	8.73×10^{-12}
20	7.08	1.95×10^7	1.55×10^{22}	22.3	1.55×10^{-11}
40	14.2	3.90×10^7	6.21×10^{22}	22.9	6.21×10^{-11}

Table C.4: COMSOL Multiphysics simulation data for model 1.3.

V_{pp} (V)	V_{rms} (V)	E (V/m)	$\nabla\|E^2\|$ (V^2/m^3)	log $\nabla\|E^2\|$	F_{dep} (N)
1	0.35	2.97×10^5	3.89×10^{18}	18.6	3.89×10^{-15}
5	1.77	1.48×10^6	9.73×10^{19}	20.0	9.73×10^{-14}
10	3.54	2.97×10^6	3.89×10^{20}	20.6	3.89×10^{-13}
15	5.31	4.45×10^6	8.76×10^{20}	21.0	8.76×10^{-13}
20	7.08	5.94×10^6	1.56×10^{21}	21.2	1.56×10^{-12}
40	14.2	1.19×10^7	6.23×10^{21}	21.8	6.23×10^{-12}

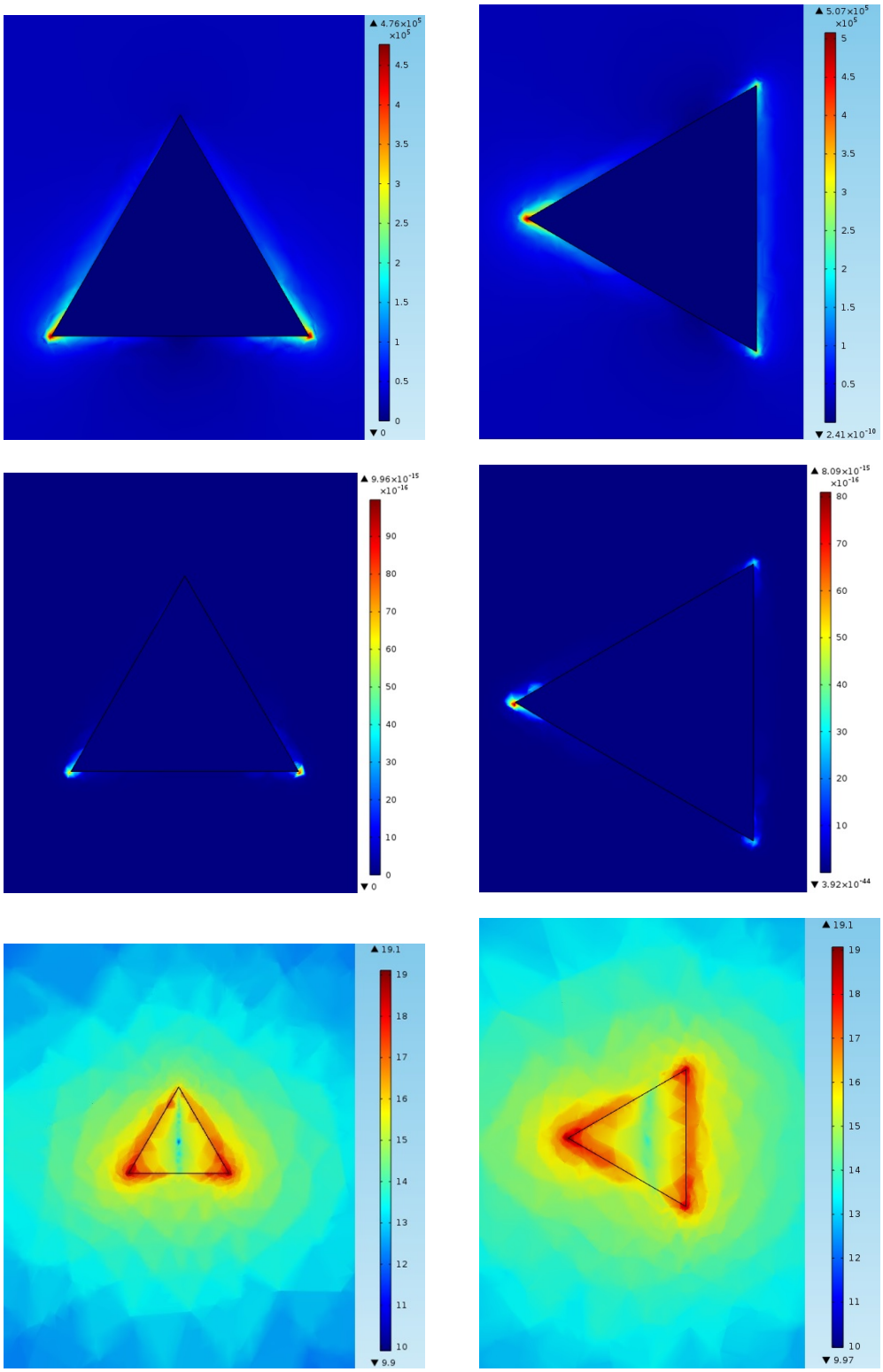

Figure C.1: Electric field, DEP force and logarithm of the gradient of the square of the electric field images for 1 V_{pp} for orientations 1 and 2 in model 1.1.

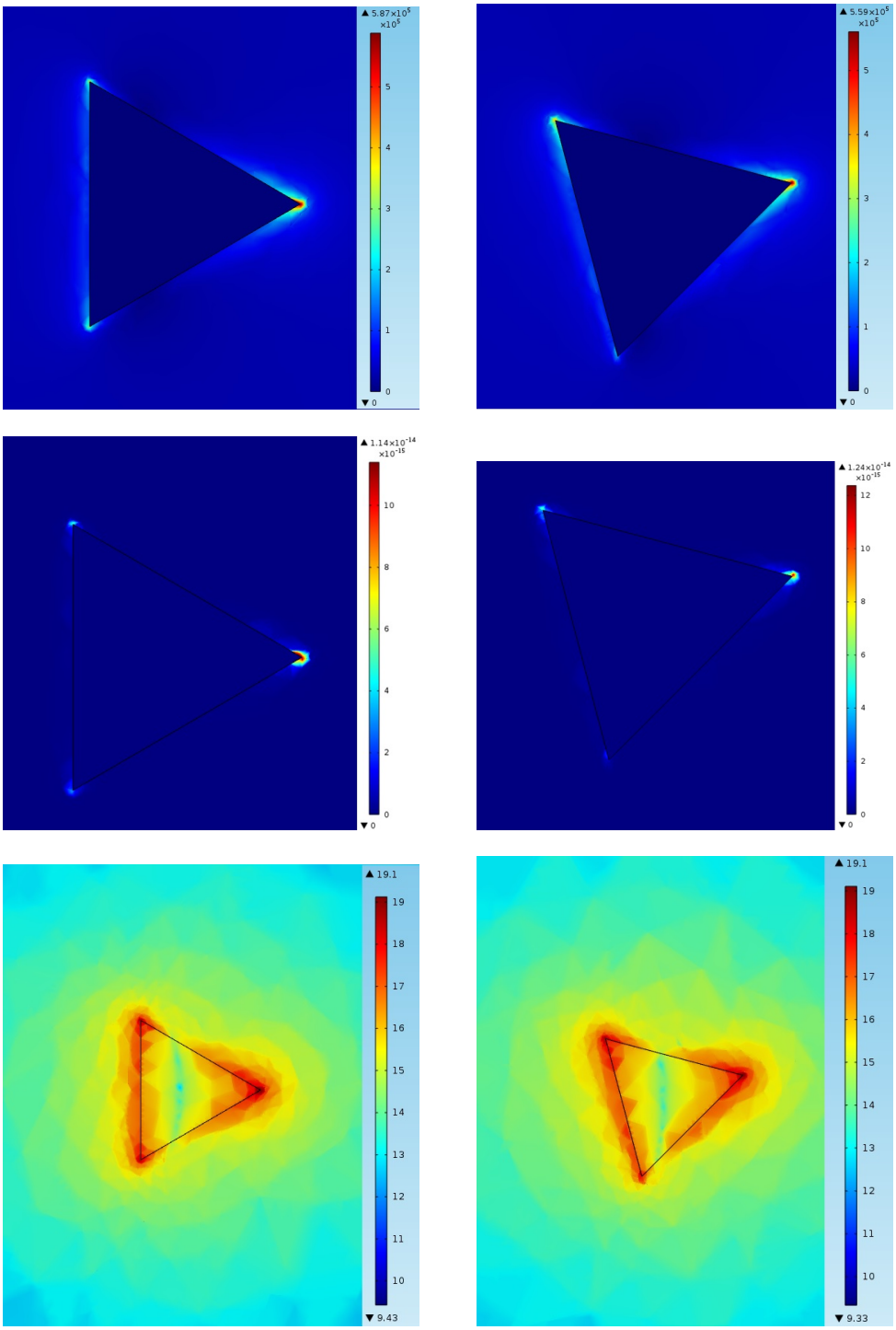

Figure C.2: Electric field, DEP force and logarithm of the gradient of the square of the electric field images for 1 V_{pp} for orientations 3 and 4 in model 1.1.

Table C.5: COMSOL data for model 2.1. Electric field, the gradient of the square of the electric field, logarithm of previous and DEP force values for different orientation with different voltages.

	V_{pp} (V)	V_{rms} (V)	E (V/m)	$\nabla\|E^2\|$ (V^2/m^3)	log $\nabla\|E^2\|$	F_{dep} (N)
electrode	1	0.35	4.53×10^5	9.79×10^{18}	19.0	9.79×10^{-15}
triangle	1	0.35	3.37×10^5	3.93×10^{18}	18.76	3.93×10^{-15}
electrode	5	1.77	2.27×10^6	2.45×10^{20}	20.4	2.45×10^{-13}
triangle	5	1.77	1.69×10^6	1.15×10^{20}	20.1	1.15×10^{-13}
electrode	10	3.54	4.53×10^6	9.79×10^{20}	21.0	9.79×10^{-13}
triangle	10	3.54	3.54×10^6	4.59×10^{20}	20.7	4.59×10^{-13}
electrode	15	5.31	6.80×10^6	2.20×10^{21}	21.3	2.20×10^{-12}
triangle	15	5.31	5.08×10^6	9.72×10^{20}	21.1	9.72×10^{-13}
electrode	20	7.08	9.06×10^6	3.91×10^{21}	21.6	3.92×10^{-12}
triangle	20	7.08	6.92×10^6	1.85×10^{21}	21.3	1.85×10^{-12}
electrode	40	14.2	1.81×10^7	1.57×10^{22}	22.2	1.57×10^{-11}
triangle	40	14.2	1.38×10^7	7.32×10^{21}	22.0	7.32×10^{-12}

Table C.6: COMSOL data for model 2.2. Electric field, the gradient of the square of the electric field, logarithm of previous and DEP force values for different orientation with different voltages.

	V_{pp} (V)	V_{rms} (V)	E (V/m)	$\nabla\|E^2\|$ (V^2/m^3)	log $\nabla\|E^2\|$	F_{dep} (N)
electrode	1	0.35	4.91×10^5	7.86×10^{18}	18.8	7.86×10^{-15}
triangle	1	0.35	7.94×10^5	2.93×10^{19}	19.5	2.93×10^{-14}
electrode	5	1.77	2.61×10^6	2.10×10^{20}	19.9	2.10×10^{-13}
triangle	5	1.77	3.97×10^6	7.33×10^{20}	20.9	7.33×10^{-13}
electrode	10	3.54	5.18×10^6	7.86×10^{20}	20.6	7.86×10^{-13}
triangle	10	3.54	7.94×10^6	2.93×10^{21}	21.5	2.93×10^{-12}
electrode	15	5.31	7.75×10^6	1.77×10^{21}	20.9	1.77×10^{-12}
triangle	15	5.31	1.19×10^7	6.60×10^{21}	21.8	6.60×10^{-12}
electrode	20	7.08	1.02×10^7	3.37×10^{21}	21.1	3.37×10^{-12}
triangle	20	7.08	1.59×10^7	1.17×10^{22}	22.1	1.17×10^{-11}
electrode	40	14.2	2.04×10^7	1.38×10^{22}	21.7	1.38×10^{-11}
triangle	40	14.2	3.17×10^7	4.69×10^{22}	22.7	4.69×10^{-11}

Table C.7: COMSOL data for model 2.3. Electric field, the gradient of the square of the electric field, logarithm of previous and DEP force values for different orientation with different voltages.

	V_{pp} (V)	V_{rms} (V)	E (V/m)	$\nabla\|E^2\|$ (V^2/m^3)	log $\nabla\|E^2\|$	F_{dep} (N)
electrode	1	0.35	3.78×10^5	4.14×10^{18}	18.8	4.14×10^{-15}
triangle	1	0.35	1.40×10^5	9.27×10^{17}	18.0	9.27×10^{-16}
electrode	5	1.77	1.89×10^6	1.03×10^{20}	20.2	1.03×10^{-13}
triangle	5	1.77	6.84×10^5	2.30×10^{19}	19.3	2.30×10^{-14}
electrode	10	3.54	3.78×10^6	4.14×10^{20}	20.8	4.14×10^{-13}
triangle	10	3.54	1.43×10^6	9.26×10^{19}	19.9	9.26×10^{-14}
electrode	15	5.31	5.67×10^6	9.31×10^{20}	21.1	9.31×10^{-13}
triangle	15	5.31	2.14×10^6	1.99×10^{20}	10.4	1.99×10^{-13}
electrode	20	7.08	7.56×10^6	1.66×10^{21}	21.4	1.66×10^{-12}
triangle	20	7.08	2.85×10^6	3.81×10^{20}	20.6	3.81×10^{-13}
electrode	40	14.2	1.51×10^7	6.62×10^{21}	22.0	6.62×10^{-12}
triangle	40	14.2	5.47×10^6	1.52×10^{21}	21.2	1.52×10^{-12}